

On the impact of heavy meson production spectra on searches for heavy neutral leptons

Jonathan L. Schubert^{1,2} Babette Döbrich² Jan Jerhot² Tommaso Spadaro³

¹*Technical University of Munich, TUM School of Natural Sciences, Physics Department, Chair for Data Science in Physics, 85748 Garching, Germany*

²*Max-Planck-Institut für Physik (Werner-Heisenberg-Institut), Boltzmannstr. 8, 85748 Garching bei München, Germany*

³*Laboratori Nazionali di Frascati dell'INFN, Via E. Fermi, 54, 00044 Frascati Italy*
*E-mail: babette@mpp.mpg.de, jan.jerhot@cern.ch,
jonathan.schubert@cern.ch, tommaso.spadaro@cern.ch*

ABSTRACT: Feebly Interacting Particles are a commonly considered extension to the Standard Model of Particle Physics. In many theoretical frameworks these particles can explain observed physical phenomena which are in tension with the current model. ALPINIST is a simplified Monte Carlo framework aimed at evaluating past, present, and future, short and long baseline experiments for their sensitivities to different models of Axion-Like Particles. We present the extension of this framework to accommodate new classes of Feebly Interacting Particles with emphasis on Heavy Neutral Leptons. This extension is especially well motivated, solving multiple of the standing issues with the Standard Model at the same time. The fundamental importance of inputs on the resulting parameter sensitivity, and thus the need for a unified simulation set-up, is highlighted.

KEYWORDS: axion, heavy neutral leptons, simulation framework, feebly interacting particles, beam-dump experiments

Contents

1	Introduction	1
2	Fixed-target phenomenology of feebly interacting particles	2
2.1	Proton beam-dump simulation of FIP searches	2
2.2	The Heavy Neutral Lepton	3
3	Heavy meson distributions at fixed-target experiments	5
3.1	Production cross section	5
3.2	Differential production cross sections	7
3.2.1	Open charmed mesons	7
3.2.2	Open beauty mesons	9
4	The ALPINIST framework	10
4.1	Axion-Like Particles in Numerous Interactions Simulated and Tabulated	10
4.2	Experiments	10
4.2.1	BEBC	11
4.2.2	NuTeV	12
4.3	Validation	13
4.3.1	Comparison to BEBC	13
4.3.2	Comparison to NuTeV	14
5	Results	16
5.1	Impact on Feebly Interacting Particle sensitivities	16
5.2	Beyond benchmark cases	18
5.3	Impact on the sensitivity landscape	19
6	Conclusions	23
A	Heavy Neutral Lepton interactions	24
A.1	Production	24
A.2	Decay	26
B	Leading particle effects on meson distributions	28
B.1	Open charmed mesons	28
B.2	Open beauty mesons	30
C	Fit details	31
D	Framework overview	33
D.1	Factorisation assumptions	33
D.2	Structural layout	34
D.3	Simulating Heavy Neutral Leptons	36

E	Further sensitivity comparisons	36
E.1	NA62 experiment in beam-dump mode	36
E.2	SHiP experiment	37
E.3	CHARM experiment	39

1 Introduction

Unlike their equivalent for Beyond Standard Model extensions at very large mass scales, which are accessible in the lab only at colliders, searches for Feebly Interacting Particles (FIPs, typically below the GeV scale) do not necessarily rely on high interaction energies [1, 2]. Instead, due to the suppressed nature of their Standard Model (SM) couplings, high intensities are required to facilitate such searches. Therefore, the FIP paradigm can be studied in a multitude of ways, including nuclear recoil for FIPs of cosmological or solar origin [3, 4], (far) displaced detection at particle colliders [5–7], and fixed-target production.¹

One of the arguably most well-motivated FIPs are Heavy Neutral Leptons (HNLs), whose discovery could help to understand the origin and scale of neutrino masses [17–19], the Dark Matter problem [20–24], and the Baryon asymmetry of the universe [25–29]. For a comprehensive overview for constraints and searches of HNLs in a wide mass region, see for example [30]. In our study we are scrutinising the phenomenology and prospects of HNL searches in proton fixed-target experiments.

In proton fixed-target experiments, a predominant production process of FIPs, and also of HNLs, is in the decay of secondary mesons originating in the primary proton shower. Specifically, it is the most boosted forward component of those mesons which is almost exclusively relevant in the computation of the FIP yield. However, since the signal from this component is typically dominated by beam induced backgrounds in fixed-target set-ups, and is thus least well known, there are uncertainties to be accounted for when modelling the production of FIP production from mesons. A detailed modelling is needed though in order to prove or disprove the existence of HNLs in data. While in decay-in-flight experiments, for example with Kaons, there is good control over the yield and kinematic distributions, the validation of the heavy meson flux is more challenging due to typically much shorter lifetimes. One of the standard tools used to model heavy meson production [31, 32] in this context is the event generator PYTHIA, other options are discussed below.

In the case of lighter mesons, an attempt [33] has been made to validate existing experimental literature against PYTHIA, such that uncertainties in shape and yield can be accounted for. For heavier mesons, this endeavour is much more difficult due to statistics [34] – a fact which has triggered projects to overcome this problem [35].

¹By referring to fixed-target experiments in this work, we refer to beam-dump [8–11], neutrino physics [12–14] and light meson decay-in-flight experiments [15, 16].

Given the heavy meson spectrum, the production, propagation and decay of HNLs can be modelled for a specific experimental set-up (c.f. figure 1). A public, unified framework is then relevant in order to reliably compare different FIP parameter reaches for different acceptance parameters (geometry, acceptance cuts...). One such tool is ALP_INIST [36, 37], originally developed for the specific case of axion-like particles. Software with similar functionality has been made available including MADDUMP [38], and more recently SENS_CALC [39], and DISPLACEDDECAYCOUNTER [40]. Such software is particularly useful for FIPs that can couple to multiple SM particles, such as HNLs, which can couple to all SM leptons. However, the relative strength of these couplings depends on the exact model at hand. Often, for simplicity, benchmark cases where the HNL couples to only one lepton are shown. With light-weight Monte Carlo (MCs) such as the ones mentioned above, a plethora of other cases can be studied easily.

In this paper we introduce a version of ALP_INIST that can handle the full production and decay chains for HNLs. In addition, we compare in detail the experimental knowledge of heavy meson production for energies relevant in proton fixed-target experiments. We compare those measurements to simulations and *scrutinise predictions for the possible discovery or exclusion of HNLs in a number of experiments*. The main focus of this version of ALP_INIST is to facilitate a public MC simulation tool to estimate (proposed) experiments for their sensitivities to the benchmark cases proposed by physics beyond colliders [1, 2].²

This paper is structured as follows: In section 2 we review the concepts of FIP searches in beam-dumps and highlight the variables interesting for the case of HNL searches. In section 3, we discuss the experimental status of heavy meson spectra in the relevant energy regimes for HNL production at beam-dumps. We compare this to state-of-the-art simulation tools. In section 4 we review the MC simulation framework ALP_INIST which will be employed to obtain sensitivity projections for a number of scenarios. Finally, we summarise the results of our studies in section 5 and discuss the impact of our study for past and future HNL searches. Lastly, we summarise our findings and discuss the relevance to other FIP cases in section 6.

2 Fixed-target phenomenology of feebly interacting particles

2.1 Proton beam-dump simulation of FIP searches

Employing a proton beam-dump in Feebly Interacting Particle searches has gained renewed interest after the last such endeavours in the 1980s. The rationale is that weakly coupled particles at MeV-GeV mass scales for a certain range of decay lengths/couplings can be accessed most sensitively.³

The general principle of a fixed-target experiment is presented schematically in figure 1 and can be summarised as follows:

²As for ALPs, the HNL implementation also allows for non-trivial combinations thereof.

³A number of subtleties have to be considered here [41], the primary one being the proper modelling of the FIPs' production, as is the main point of this article.

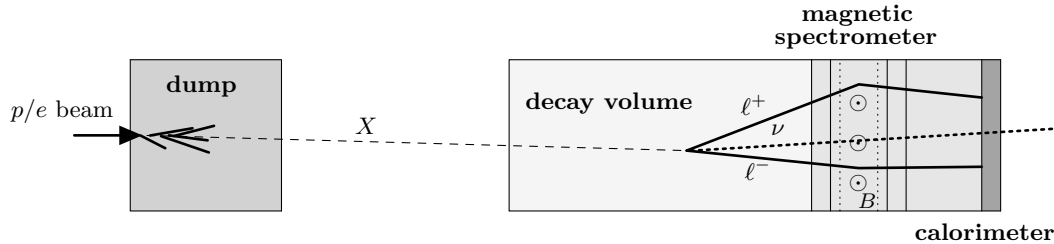


Figure 1. Schematic layout of a typical beam-dump experiment.

1. A highly energetic beam particle impinges on a stationary target (dump) and scatters off the material.
2. A feebly interacting particle X is produced in primary or secondary interactions of the beam particle with the dump material with a probability χ_X
3. Due to its inherently limited interaction strength, X is assumed to propagate freely up to the point of its eventual decay.
4. With a given probability P_{FV} , the decay of X occurs in a fiducial decay volume.
5. With a given probability P_{acc} , the SM decay products of X are within the acceptance of a detector apparatus.

For a generic FIP with mass m_X and SM coupling g_X , the number of detectable events with a given final state can thus be estimated as

$$N_{\text{evt}}(m_X, g_X) = N_{\text{PoT}} \chi_X(g_X, m_X) P_{\text{FV}}(m_X, \Gamma_X) \epsilon_{\text{det}} P_{\text{acc}}(m_X), \quad (2.1)$$

where N_{PoT} is the number of beam particles on target, $\Gamma_X(g_X, m_X)$ is the width of X , and ϵ_{det} quantifies the detection probability of the final states crossing the detectors. As nearly all beam particles will interact with the dense material of the dump, beam-dump experiments typically feature a very high luminosity compared to collider experiments, albeit at an inherently lower centre-of-mass energy. This makes them the ideal class of experiments to look for FIPs, as the FIPs' very small interaction cross sections can be compensated by the high luminosity.

2.2 The Heavy Neutral Lepton

In this section we will outline the steps in simplifying the fixed-target phenomenology of the HNL into a tabulation-compatible framework. The HNL is commonly introduced as part of the type-I seesaw, where \mathcal{N} new right chiral singlet fermions ν_{RI} featuring a Majorana mass M_I are added to the content of the SM Lagrangian [17, 18]. These states can couple to the SM ‘active’ neutrinos $\nu_{L\alpha}$ of lepton generation α via a Yukawa-like term which after electroweak symmetry breaking yields

$$\mathcal{L}_{\alpha I}^{\nu_L \nu_R} = - (F_{\alpha I}^{\nu})^* \frac{v}{\sqrt{2}} \nu_{L\alpha}^{\dagger} \nu_{RI} + h.c. \quad (2.2)$$

Here, $F_{\alpha I}$ denotes the Yukawa coupling of the I -th right chiral singlet to lepton generation α , and v is the Higgs' vacuum expectation value. Diagonalising in the mass basis yields \mathcal{N} heavy Majorana states (HNLs) N_I with masses m_{N_I} .⁴ Consequently the HNL inherits couplings to SM fields from its left chiral component, namely

$$\mathcal{L}_{\text{int}} = \frac{g}{2\sqrt{2}} W_\mu^+ \sum_{\alpha, I} \theta_{\alpha I}^* \bar{N}_I^c \gamma^\mu (1 - \gamma_5) \ell_\alpha^- + \frac{g}{4 \cos \theta_W} Z_\mu \sum_{\alpha, I} \theta_{\alpha I}^* \bar{N}_I^c \gamma^\mu (1 - \gamma_5) \nu_\alpha + h.c. \quad (2.3)$$

where the interactions are suppressed by the mixing angles

$$\theta_{\alpha I} \equiv \frac{F_{\alpha I} v}{\sqrt{2} M_I}. \quad (2.4)$$

For simplicity in phenomenological studies, the HNLs are commonly approximated by a single fermion N with mass m_N , and mixing angles θ_α which is either Majorana or Dirac in nature. It is further convenient to define the *coupling suppression* $U_\alpha^2 = |\theta_\alpha|^2$, which in the following we will often refer to simply as the coupling. This allows us to simplify the parameter space from $7\mathcal{N} - 3$ free parameters in the full HNL theory to the HNL mass, the set of (U_e, U_μ, U_τ) and the choice between Majorana or Dirac type HNL. For recent reviews, please see [2, 42] and references therein.

In accordance with eq. (2.3), HNLs can appear and decay through weak interactions at a suppressed rate (determined by U_α^2). Thus, possible production mechanisms at beam-dump facilities include i) deep inelastic and coherent proton-nucleus scattering processes, and ii) the (semi-) leptonic decay of secondary mesons and τ leptons. In this work we will limit ourselves to the production through ii), as this contribution typically outweighs mechanism i) by several orders of magnitude for the typical centre-of-mass energies of fixed-target experiments [43]. We further assume that the HNL does not couple to lighter dark sector particles, so that its width is purely determined by the decays allowed by the interactions prescribed by eq. (2.3).

The theoretical description of heavy neutrinos regarding their production in meson decays and decay channels has long been established in literature [44–46] and is mostly consistent with more recent reviews dedicated to HNLs [47, 48]. A crucial difference however, are the contributions of neutral current interaction to some final states of the HNL decay, which can lead to significant discrepancies in terms of phenomenological implications [49, 50]. We consider width contributions to the HNL with a mass up to the B_s mass as listed in the most recent review on the subject [43] with updated underlying theory inputs as listed in appendix A. This leads to slightly different branching ratios for three-body decays of beauty mesons which are shown for an electronphilic HNL in figure 14. A brief summary of the production and decay widths are listed for the reader's convenience in appendix A.

⁴Additionally, this yields three light Majorana neutrinos with masses m_{ν_i} determined by the seesaw relation $\left(V_{\text{PMNS}}^\dagger \text{diag}(m_{\nu_1}, m_{\nu_2}, m_{\nu_3}) V_{\text{PMNS}} \right)_{\alpha\beta} \simeq -v^2 \sum_I \frac{F_{\alpha I} F_{\beta I}}{M_I^2} m_{N_I}$.

3 Heavy meson distributions at fixed-target experiments

In the 100 MeV to few GeV mass range, where beam-dump searches dominate, HNLs are most abundantly produced in the decays of charm and beauty mesons (see section 2.2 and appendix A). Thus, it is paramount to accurately describe the meson production in order to evaluate the resulting HNL distributions and eventual detector responses. This not only extends to the production probability of the meson, but importantly also to their kinematic spectra, as we will see in this section.

The simulation package PYTHIA is one of the tools most used in the community to determine the expected yield of mesons produced by proton interactions, e.g. [51–53].

3.1 Production cross section

The most straightforward way in which meson properties affect the production of Feebly Interacting Particles is through the meson production cross section, determining how many mesons and therefore potential decays into FIPs we observe. For heavy mesons this is commonly quantified by the pair production cross section of the relevant heavy valence quark $\sigma_{q\bar{q}}$. The production rate of a given meson is then determined by the convolution of the quark level cross section and fragmentation functions subject to the QCD environment around the heavy quarks [34].

These cross sections can be calculated from the theory side. PYTHIA provides an internally generated estimate for $\sigma_{q\bar{q}}$. However, these are known to underestimate the measured cross sections, prompting often a naive rescaling of the estimate by a factor $k_{q\bar{q}}$ typically of the order few [34, 51]. Alternatively, the cross sections can be calculated directly in various schemes using pQCD (e.g. massive quarks at NLO [54]), with one of the most widely used schemes being the fixed order next-to-leading logarithm (FONLL) approach [55, 56]. To calculate the production cross section, we employ the FONLL software interfaced with LHAPDF6 [57] to use the NNPDF4.0 proton parton distribution functions [58].

On the experimental side, the open charmed (or D) mesons feature a variety of relatively clean decay signatures, and a sizeable production cross section even at typical energies for beam-dump experiments. Notably, charm decays affect significantly the energy spectrum of neutrinos emitted at these centre-of-mass energies, which gave a motivation for several experiments in the past to accurately measure the charm production cross section (see e.g. [59] for a review). For open beauty (or B) mesons, however, the production cross section at centre-of-mass energies around 30 GeV is smaller than for charmed mesons by three orders of magnitude. No experimental data is available for centre-of-masses below 40 GeV.

We use the PyMC Gaussian Process [60] to perform a Bayesian fit to the data (see appendix C for details). The posterior distribution is calculated as a marginal likelihood using the central value and the estimated error of the FONLL calculation as a prior. The resulting posterior shows a good agreement with the FONLL calculations within the respective uncertainties, as shown in figure 2. The fit results for relevant beam energies of

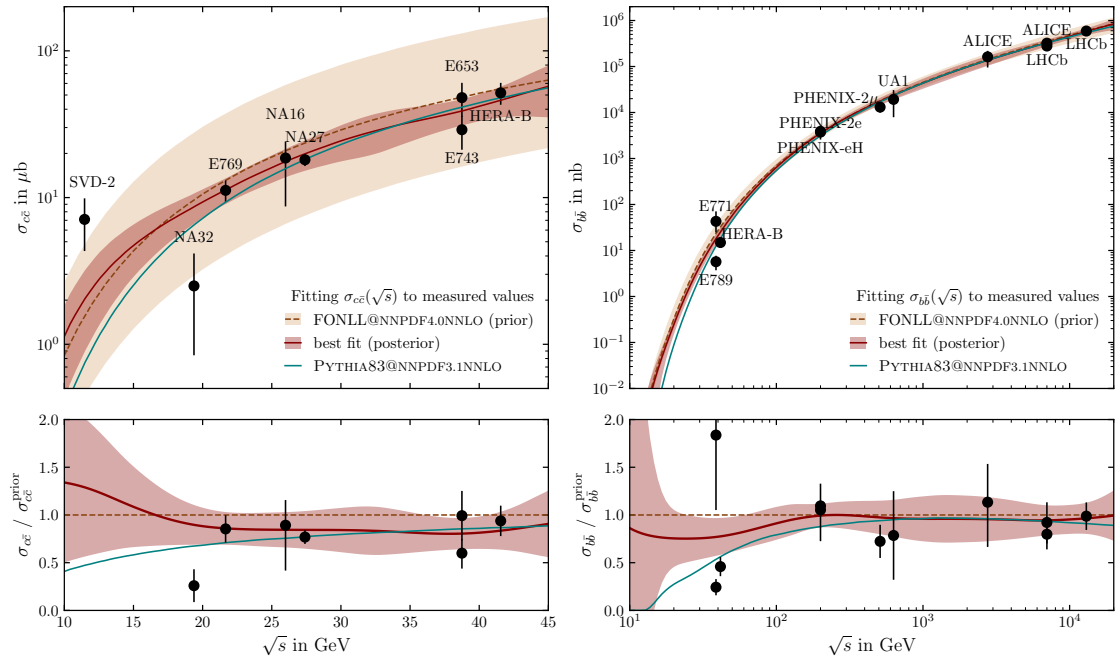


Figure 2. Charm (left) and beauty (right) pair production cross sections as a function of the centre-of-mass energy of the pp collision. The FONLL calculation [55, 56] (dashed brown curve with orange filled area showing the uncertainties from scale and quark mass variation), the Bayesian fit to the data [61–78] (red curve with light-red filled area showing the 68%, CL), and the PYTHIA calculation (teal curve), scaled by a factor $k_{q\bar{q}}$ obtained through an ODR fit to the data are compared. The lower panels show the production cross section normalised to the central value predicted by the FONLL calculation. For further details see text.

different beam-dump facilities are summarised in table 1, with further information about the fit in appendix C.

In figure 2 we also compare the Bayesian fit to the PYTHIA result⁵ scaled by a multiplicative constant $k_{q\bar{q}}$ determined by an orthogonal distance regression (ODR) fit to the data. We find that at the higher end of the centre-of-mass energies presented, the scaled PYTHIA curve agrees reasonably well with both the fit result and the FONLL calculation. Especially at the lower end of the \sqrt{s} spectrum, the PYTHIA curve significantly underestimates the production cross sections for both charmed and beauty quarks. For $\sigma_{b\bar{b}}$, data points at much higher energy scales are included to achieve a more stable extrapolation and the fit is performed on $\log(\sqrt{s})$. Nonetheless, the diverging uncertainty at $\sqrt{s} \rightarrow 0$ reflects the absence of data and cannot be avoided.

Unless otherwise stated, the production cross sections for the various beam-dump experiments considered in this work are the fit results listed in table 1.

⁵This result was derived using the most up to date NNPDF proton parton distribution function available in PYTHIA 8.3, the NNPDF3.1 NNLO+LUXQED [58].

E_{beam} in GeV	$\sigma_{c\bar{c}}$ in μb	$\sigma_{b\bar{b}}$ in nb
70	2.2 ± 1.2	–
120	4.6 ± 1.8	0.02 ± 0.02
400	20.0 ± 4.5	2.63 ± 0.76
800	39.5 ± 7.7	18.6 ± 4.6

Table 1. Best fit results for quark anti-quark pair production cross sections $\sigma_{q\bar{q}}$ for typical beam energies E_{beam} at beam-dump facilities.

3.2 Differential production cross sections

Another important aspect about mesons regards their kinematic spectra, as these greatly impact the kinematic spectra of their eventual FIP daughters. The meson spectra are usually given in terms of the Feynman parameter x_F quantifying the centre-of-mass momentum transfer of the beam to the meson ($x_F = p_z^{\text{CM}}/p_{z,\text{max}}^{\text{CM}-1}$) and p_T , the momentum orthogonal to the incident beam axis’ modulus. A common way to parameterise the differential cross section of heavy mesons in a fixed-target experiment is given by [34]

$$\frac{\partial^2 \sigma}{\partial x_F \partial p_T^2} \propto (1 - |x_F|)^n e^{-(ap_T + bp_T^2)}, \quad (3.1)$$

which we will use in the following to summarise different measurement results. It is important to note that heavy meson decay lengths are typically orders of magnitude below the typical material interaction lengths, justifying a prompt decay assumption.⁶ Therefore, the following considerations are valid on the nucleon level irrespective of the target material.

3.2.1 Open charmed mesons

Many of the experiments that measured the total production cross section also made an effort to measure their differential distributions. A summary of the experimental information is listed in table 2. Large uncertainties and significantly differing power laws are obtained by different experiments. As we will see in section 5.1, such differences are relevant for the sensitivities of searches for HNLs. Using the data presented in table 2, we employ a similar Bayesian fitting procedure as presented in section 3.1. As a theory motivated prior for these fits, we use PYTHIA 8.3 to generate meson spectra to which we then fit eq. (3.1) using orthogonal distance regression. As most of the experimental data in table 2 is presented with $a = 0$ and b as a free parameter to fit the measured p_T distribution, we follow this convention. The b fit results on the PYTHIA generated data consistently underestimate the experimental results. Therefore, we decided to scale the prior b value by a global factor of 2. In the absence of a theory motivated uncertainty, we apply a prior 68% CL region as $\pm 50\%$ with respect to the central prior value. The resulting band covers almost all of the data uncertainty ranges.⁷

⁶The longest living heavy meson is the B^\pm meson with a life time equivalent to $c\tau_{B^\pm} = 491(1) \mu\text{m}$. Meanwhile, the nuclear interaction lengths in copper (153.2 mm) or lead (175.9 mm) are orders of magnitude longer. [79]

⁷This is not the case for 2 of the 5 data points for the $b_{c\bar{c}}$ fit, resulting in the poor expected log point wise predictive density score presented in table 6.

experiment	target material	E_{beam} [GeV]	n	a [GeV $^{-1}$]	b [GeV $^{-2}$]
ACCMOR(NA32)	Si	200	$5.5^{+2.1}_{-1.8}$	–	$1.4^{+0.6}_{-0.4}$
WA82	Cu	370	6 ± 0.3	–	0.93 ± 0.09
LEBC-EHS(NA27)	H ₂	400	4.9 ± 0.5	–	0.99 ± 0.09
CHARM	Cu	400	$6.2^{+0.4}_{-0.5} \pm 0.4$	2.0 ± 0.3	–
LEBC-MPS(E743)	H ₂	800	8.6 ± 2.0	–	1.1 ± 0.3
E653	emulsion	800	$6.9^{+1.9}_{-1.8}$	–	$0.84^{+0.10}_{-0.08}$
HERA-B	C, Ti, W	920	7.5 ± 3.2	–	–

Table 2. Experimental results [62, 64, 67–69, 80, 81] for the differential cross section measurements of open charmed meson production in proton beam fixed-target interactions as parameterised by eq. (3.1).

The results of this fit are shown in figure 3 and summarised for common beam-dump energies in table 3. We find that $n_{c\bar{c}}^{\text{PYTHIA}}$ (ODR fit results of the PYTHIA spectra) agrees reasonably well with the data. The fact, that $b_{c\bar{c}}^{\text{PYTHIA}}$ consistently underestimates the data points means that PYTHIA overestimates the multiplicity of events featuring large p_T . For FIP searches with far away on-axis detectors this would result in underestimating the signal, due to disproportionately many FIPs inheriting the larger p_T tendency and going out-of-acceptance.

E_{beam} in GeV	$n_{c\bar{c}}$ in μb	$b_{c\bar{c}}$ in GeV $^{-2}$
70	3.6 ± 2.0	1.66 ± 0.54
120	4.4 ± 1.6	1.41 ± 0.40
400	5.81 ± 0.28	0.96 ± 0.06
800	7.29 ± 0.95	0.85 ± 0.08

Table 3. Best fit results for differential cross section as parameterised by eq. (3.1) at $a = 0$ for typical beam energies E_{beam} at beam-dump facilities.

In the above, we have considered all open charmed mesons to follow the same differential distributions. While most of the experiments do not consider a unique differential cross section for the different possible charm flavours (D^+ , D^- , D^0 , ...), LEBC-EHS (NA27) attempted to identify different curves for the different flavours. This is motivated by an expected contribution to the production cross sections of the *leading particle effect*, possibly including “2 \rightarrow 3” parton processes (heavy recombination). The underlying principle of this phenomenon is that spectra of secondary particles sharing a valence quark with the beam particle are harder with respect to their charge conjugate counterparts which do not have such a valence quark in common.

The different meson spectra would consequently not only impact the distribution of FIPs by virtue of their production mechanism being meson dependent (i.e. decay channels of D^\pm do not necessarily exist for D^0 with the same kinematics), but also yield different spectra for

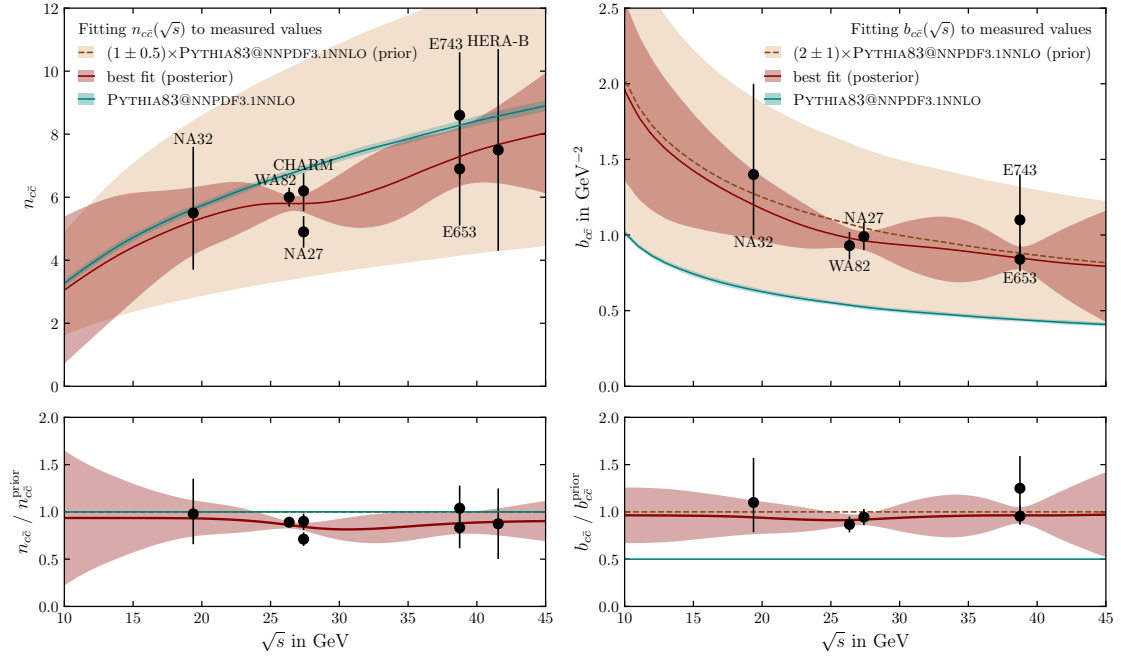


Figure 3. Charm differential cross section parameters of forward (left) and transversal (right) momentum as parameterised by eq. (3.1) at $a = 0$ pair production cross sections as a function of the centre-of-mass energy of the pp collision. The PYTHIA results are derived using an ODR fit of eq. (3.1) at $a = 0$ to the spectra generated with PYTHIA 8.3. The scaled PYTHIA calculation (dashed brown curve with orange filled area showing assumed prior uncertainty), the Bayesian fit to the data [62, 64, 67–69, 80, 81] (red curve with light-red filled area showing the 68%, CL), and the unscaled PYTHIA (teal curve with teal area showing the fit uncertainty). The lower panels show the respective parameters normalised to the scaled central values derived from the PYTHIA spectra (prior). For further details see text.

(anti)-HNLs in case of Dirac-like HNLs.⁸ Our present understanding is that the real impact on the differential cross section of the leading particle effect in proton-nucleon collisions at the energy scales of beam-dump experiments is as of yet experimentally inconclusive. However, the interested reader can find a brief summary in appendix B. Nevertheless, the fit presented in this section can be seen as an envelope for the individual distributions of open charmed mesons.

3.2.2 Open beauty mesons

For beauty mesons the experimental landscape in terms of production (differential) cross sections for fixed-targets in the relevant energy range is even more sparse than for their charmed counterparts. Therefore, no attempt was made at validating the spectra generated with PYTHIA 8.309. Nonetheless, the interested reader can find a brief summary of the impact of possible future PYTHIA extensions in appendix B.2.

⁸Furthermore, this would greatly impact the oscillation patterns which could be observed for example in the pseudo-Dirac-limit for two HNLs. [82–84]

4 The ALPiNIST framework

In order to study the effects of a multitude of different input assumptions on the expected sensitivities of various past, present, and future experiments to Feebly Interacting Particles, we make use of the Axion-Like Particle in Numerous Interactions Simulated and Tabulated (ALPiNIST) simulation framework [36, 85]. In this section we will give a brief overview of the framework (section 4.1), introduce the experiments that are already implemented for simple simulations (section 4.2), and briefly outline a validation of the set up (section 4.3).

4.1 Axion-Like Particles in Numerous Interactions Simulated and Tabulated

The ALPiNIST framework was originally implemented to facilitate the study of parameter reach of different fixed-target experiments (beam-dumps) to Axion-Like Particles with various coupling structures [36, 37]. The updated version, published together with this work⁹, has been extended by several different models of Feebly Interacting Particles, covering all the PBC benchmark cases [1, 2], which can now be studied in a unified MC simulation set-up. The general layout of the simulation framework (shown in figure 20 and discussed in section D.2) is closely related to the general layout of beam-dump experiments (see section 2) separating production and detection of the FIP. The central idea of this simulation workflow, is that the kinematic and model-dependent part can, to a large extent, be separated (see section D.1). Using common input and theory assumptions, and levels of abstraction, experiments can then be compared on an even footing.

4.2 Experiments

The ALPiNIST framework features an abstraction scheme of fixed-target experiments, classifying them by common features. These defining features are

E_{beam} the beam energy

N_{PoT} the number of beam particles on target

M the target material and associated material constants

l_{DV} the length of the decay volumes (for neutral l_n and charged l_c final states)

z_{DV} the distance of the decay volume from the target

θ_{off} the angular offset with respect to the beam axis

z_{Ecal} the distance of the electromagnetic calorimeter from the target

For some experiments, the quantities z_{Spect} (the distance of an eventual spectrometer from the target) and z_{MuV} (the distance of an eventual muon ID system from the target) are also relevant. Using z_{Ecal} and the calorimeter’s orthogonal geometry, one can determine the solid angular coverage Ω_{cov} which gives a figure of merit for an experiment’s geometric acceptance. These values are listed in table 4 for experiments already implemented in the ALPiNIST framework. This highlights the versatility of the ALPiNIST approach, where

⁹Available on Github under github.com/jjerhot/ALPiNIST.

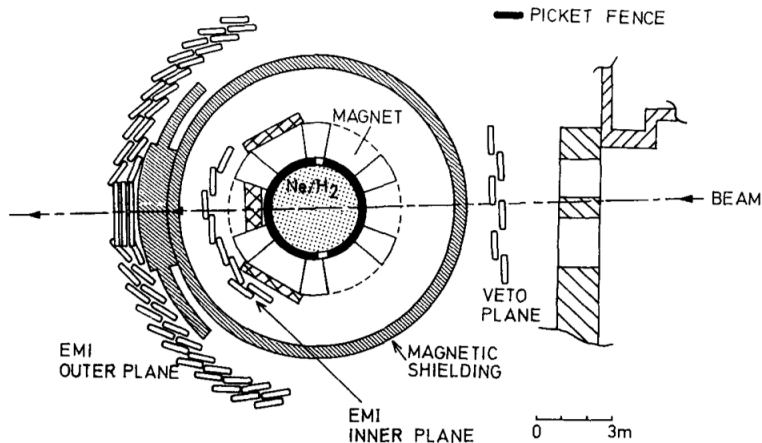


Figure 4. The BEBC chamber and detector array as adapted from [87].

extremely near (DarkQuest) and long baseline (NuTeV) experiments, and different beam energies spanning more than an order of magnitude can be simulated in a unified set-up.

The implementation of the NuCal, NA62/HIKE, DUNE ND, DarkQuest, and KOTO experiments were already described in detail in previous works [36, 37]. The geometries of the SHiP and SHADOWS experiments were updated in order to match the design changes as presented in the respective technical proposals [8, 9], which brought significant changes to the SHiP experimental layout in order to adjust to its new housing facility (CERN cavern ECN3, see also appendix E.2). The newly added BEBC and NuTeV experiments will be introduced in more detail below.

4.2.1 BEBC

The Big European Bubble Chamber (BEBC) was a 35 m^3 hydrogen bubble chamber set up in the CERN West Area, hosting a wealth of different experiments [86]. In this context we refer to the WA66 experiment, which took data during the 1982 CERN SPS beam-dump run [87]. The centre of the chamber was aligned with the beam axis and located 405.9 m downstream from the front of the dump. The detector set-up is shown in figure 4 and consists of a veto plane reducing backgrounds due to upstream muons, the chamber in the centre which acts as both decay volume and tracker simultaneously, and the external muon identifier inner and outer plane. The chamber was, further, surrounded by proportional tubes and equipped with two solenoids in Helmholtz arrangement generating a central magnetic field of 3.5 T [88, 89]. These were neglected in the ALPiNIST model of BEBC, as they have negligible impact on the cuts applied on true MC events. Changes to the decay probability due to the Ne/H₂ mixture in the chamber were also neglected. To ‘optimise the event rate and the measurability of tracks’, the fiducial volume was limited to a 16.6 m^3 $6.2\text{ mrad} \times 8.8\text{ mrad}$. In ALPiNIST we approximate this by a ($r = 1.25\text{ m}$, $h = 3.55\text{ m}$) cylinder which is concentric and coaxial with the bubble chamber.

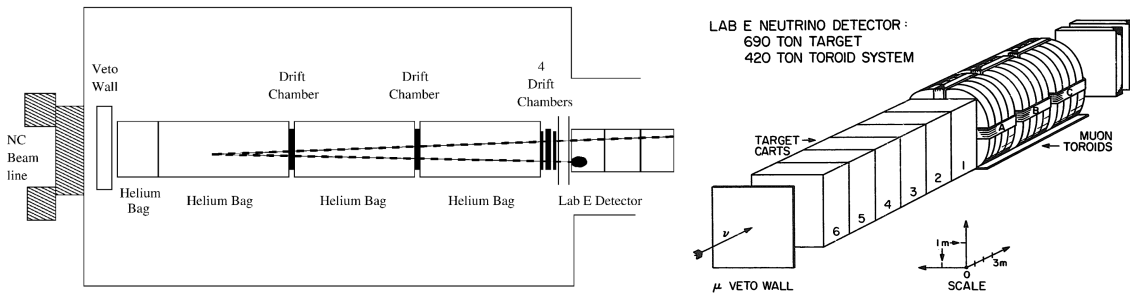


Figure 5. The NuTeV decay and tracking (left) and particle identification (right) array as adapted from [90, 92].

4.2.2 NuTeV

The Neutrinos at TeVatron (NuTeV) or E815 experiment was located at the Fermilab National Accelerator Laboratory’s Tevatron and dedicated to the study of neutrinos. During the fixed-target run, 2.54×10^{18} protons were dumped into a BeO target at an energy of 800 GeV. At 1.4 km downstream from the target, a detector set-up as depicted in figure 5 was used to study the produced neutrinos and their interactions, but also provided excellent sensitivity to muonphlic HNLs. This array consisted of a veto wall to reduce upstream backgrounds, several drift chambers interspaced in the decay chamber facilitating the tracking of charged decay or interaction products, and a 690-ton iron-scintillator sampling calorimeter followed by a toroidal muon spectrometer [90, 91]. The decay volume was further filled with helium bags which were not included in the ALP*N*IST model.

Experiment	Status	E_{beam} [GeV]	N_{PoT} [10^{18}]	Target	$l_{\text{n,DV}}$ [m]	$l_{\text{c,DV}}$ [m]	z_{DV} [m]	θ_{off} [mrad]	Ω_{cov} [μsr]
CHARM	completed	400	2.4	Cu	35	35	480	10	34
BEBC	completed	400	2.72	Cu	2.5	2.5	404	0	53
NuCal	completed	70	1.7	Fe	23	23	64	0	700
NuTeV	completed	800	2.54	BeO	34	34	1400	0	4.3
NA62	running	400	1	Cu	139	81	82	0	84
KOTO	running	30	2.2	Au	3.1	3.1	23.9	280	4300
DarkQuest-I	in prep. [93]	120	1.44	Fe	13.5	1	5	0	12000
DarkQuest-II	in prep. [93]	120	100	Fe	13.5	7	12	0	12000
DUNE ND	in prep.	120	1100	C	10	10	575	0	36
SHiP	in prep.	400	600	Mo	60.5	50	33.5	0	3900
HIKE	rejected [94]	400	15	Cu	139	81	82	0	84
SHADOWS	rejected [94]	400	15	Cu	23	20	10	69	4800

Table 4. Simplified geometries of several experiments assumed in ALP*N*IST, as well as their respective statuses.

4.3 Validation

The kinematic treatment of the ALP_INIST simulation framework has already been studied extensively in previous works [36, 37]. A natural way to validate that the set-up is compatible with the simulation of HNLs is a comparison to previously published data, which will be the main focus of this section.

4.3.1 Comparison to BEBC

One of the most stringent limits on HNL mixing parameters in the mass regime around $m_N \simeq 1$ GeV comes from the WA66 experiment at the Big European Bubble Chamber using the CERN west area beam-dump [95]. The original analysis searched for electronphilic and muonphilic HNLs produced in the two-body decays of D^\pm mesons, and decaying only via charged current interactions, and was later recast as limits for tauphilic HNLs decaying also in neutral current interactions [96]. Using the simplified geometry as described in section 4.2.1, the BEBC results were interpreted in the ALP_INIST framework.

In an effort to recreate the published exclusion limits, we assumed HNL production from the decays $D^\pm \rightarrow \ell^\pm N$ with a D meson spectrum parameterised by eq. (3.1) with $n = 4$, $a = 2$, $b = 0$. In the original search, the D meson spectrum was normalised to the measured neutrino flux. As the numerical value of the normalisation was not published, we use instead the $\sigma_{c\bar{c}} = 15.1 \mu\text{b}$ production cross section as measured by the LEBC-EHS collaboration [66], including a cascade production factor of 2.3 in accordance with cascade evaluations by the SHiP collaboration [51]. Consequently, the produced HNLs within geometric acceptance of BEBC were allowed to decay in charged current interactions. On the resulting final products the kinematic cuts as performed by the WA66 search were applied. These can be summarised in natural units as

1. $1 \text{ GeV} < \sum p_{\text{track}}$
2. $0.8 \text{ GeV} < p_{\text{track}}^e$, and $3 \text{ GeV} < p_{\text{track}}^\mu$
3. $p_T + \sqrt{p_T^2 + M_{\text{vis}}^2} < m_{D^\pm} - m_\ell$,

where p_{track} is the total momentum associated with a charged track, c the speed of light, M_{vis} is the invariant mass of the charged tracks and p_T the modulus of their combined momentum transverse to the beam direction. The limit determined by the D^\pm (m_{D^\pm}), and lepton mass (m_ℓ) are chosen depending on which lepton family the HNL couples to. Requiring the minimum momenta for the charged tracks results in combined detection and identification efficiencies of 89 % for final states including two muons, and else 88 %.

Figure 6 compares the published data by the WA66 collaboration [95] to the recast performed with ALP_INIST in terms of an electronphilic (left) and muonphilic (right) HNL produced only in $D^\pm \rightarrow N\ell^\pm$, and decaying only to $\nu\ell\bar{\ell}$, $\nu\ell\bar{\ell}'$, and $\pi\ell$ and charge conjugate processes, where ℓ is a light lepton (e and μ). The curves correspond to a parameter exclusion at 90 % CL, where the confidence level is evaluated with one event having been observed after cuts with 0.6 expected background events for the muonphilic HNL, while for the electronphilic HNL no such event was observed. The recast reproduces the published

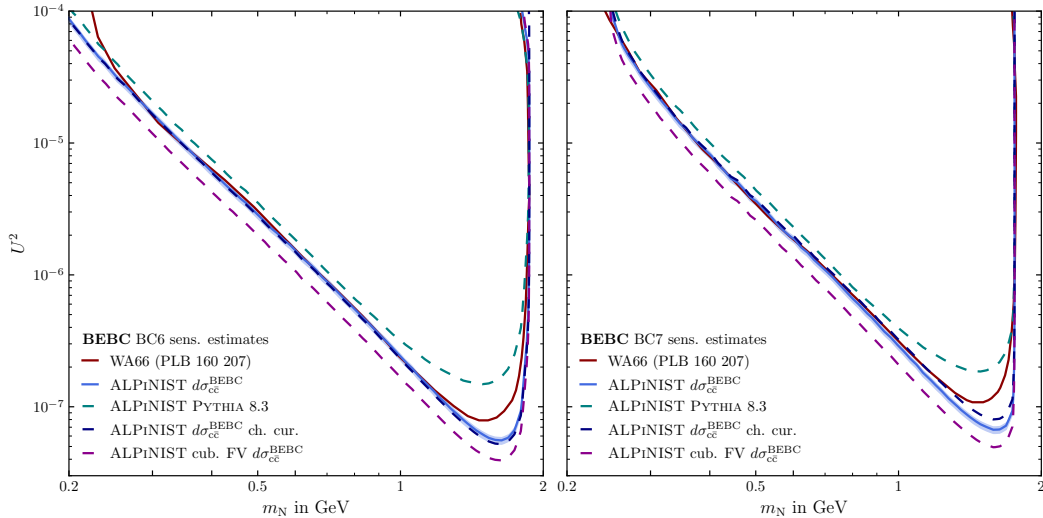


Figure 6. BEBC published (red) and ALPiNIST recast exclusion bounds for an electronphilic (left) and muonphilic (right) HNL produced in $D^\pm \rightarrow N\ell^\pm$, and decaying to $\nu\ell\ell$, $\nu\ell\ell'$, and $\pi\ell$. The blue curves were generated using charmed meson distributions quoted by WA66 as input. The dark blue dashed curve shows an HNL only decaying in charged currents, while for the light blue also neutral current interactions are permitted. The teal dashed curve uses meson inputs generated with PYTHIA’s `HardQCD:hardccbar` in standard settings. The magenta dashed curve uses a cuboid fiducial volume, as proposed in a recent recast of the BEBC results [96]. For further assumptions please find the surrounding text.

curves very well for most of the covered parameter space. Disagreements can be observed for both benchmark cases at the upper mass end of the kinetically allowed region, where ALPiNIST shows a slightly more optimistic sensitivity. For the electronphilic case, the two curves also diverge at the lowest masses presented, where the published sensitivity drops significantly when approaching the dimuon threshold. This is unexpected, as this threshold should not correspond to a significant kinematic limit for the electronphilic case. In both cases, using PYTHIA generated kinematic distributions as the D^\pm meson inputs (teal dashed curve) leads to a less restrictive exclusion bound. The magenta dashed curve represents the same assumptions as the blue curve, but instead employs a cuboid fiducial volume, as proposed in a recent recast of the BEBC results [96]. Lacking information about the uncertainties of the meson distribution used by BEBC, we varied only the overall scaling according to the neutrino flux uncertainty of 14% in accordance with values cited by the CHARM experiment [97] which shared the same target resulting in the blue band. We see that the cuboid approximation yields a more optimistic parameter reach compared to the smaller cylindrical fiducial volume implemented in ALPiNIST.

4.3.2 Comparison to NuTeV

The most recent search for HNLs at a beam-dump facility comes from the NuTeV collaboration [92], which focused on HNLs mixing with the SM muon neutrino. This analysis was implemented in ALPiNIST using the simplified geometry described in section 4.2.2. To

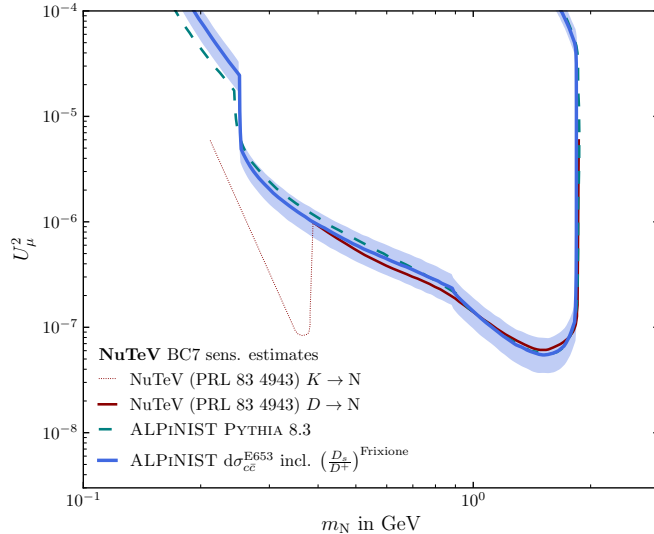


Figure 7. NuTeV published (red) and ALPiNIST recast exclusion bounds for a muonphilic HNL. The blue curve was generated using E653 charmed meson distributions [68] as input, and varying the relevant values within their 1σ bounds. The teal dashed curve uses meson inputs generated with PYTHIA’s `HardQCD:hardccbar` in standard settings.

reproduce their findings we assume the production cross section ($\sigma_{c\bar{c}} = 76 \mu\text{b}$) and meson distributions (parameterised by eq. (3.1) with $n = 6.8$, $a = 0$, $b = 0.81$) as measured by the E653 experiment [68].¹⁰ We further assumed the same kinematic distribution for D_s mesons using the $D_s(D^+ + D^0)^{-1}$ ratio of 0.2 as given by the cited theory reference [59]. Finally, we apply the full kinematic cuts on the final decay products as listed by the NuTeV search [92]. For this we define, E_{track} as the energy of final state particles, the visible final states’ invariant mass M_{vis} and total transverse momentum p_T , the missing energy E_{miss} , and the momentum transfer to the hardest final state muon Q_{vis} . The cuts can then be summarised as

1. $2 \text{ GeV} < E_{\text{track}}^\mu$, and $10 \text{ GeV} < E_{\text{track}}^e, E_{\text{track}}^\pi$
2. $M_{\text{vis}}^2 \times (2m_p Q_{\text{vis}})^{-1} < 0.1$
3. $m_p^2 + 2m_p E_{\text{miss}} - Q_{\text{vis}}^2 > 4.0 \text{ GeV}^2$
4. $p_T + \sqrt{p_T^2 + M_{\text{vis}}^2} < 3.0 \text{ GeV}$,

in natural units, where m_p is the proton mass.

Figure 7 shows the comparison of the published data by the NuTeV collaboration [92] to the recast performed with ALPiNIST in terms of a muonphilic HNL, which was evaluated for the final states $\nu e \mu$, $\nu \mu \mu$, $\pi \mu$, and $\rho \mu$. The curves show the HNL parameter exclusion at

¹⁰The discrepancy between the cross sections measured in the emulsion [68] and bubble chamber [67] experiments may highlight the importance of including cascade effects to the production cross section as presented in ref. [51].

90%CL. In accordance with the NuTeV results, we assume no data event after cuts with an expected background of 0.57 events. Below ~ 400 MeV, the NuTeV sensitivity is dominated by HNLs produced in Kaon decays. As described in appendix A, we do not consider this production channel, which is why the curves diverge. Above this threshold, however, the curves agree well. We also present the uncertainties of the experimental inputs by varying the input parameters in the listed confidence levels, shown as the blue band. Lastly, we ran the same simulation set-up with inputs coming from PYTHIA’s `HardQCD:hardccbar`. This is shown as the green dashed curve and agrees well with the published curve near the kinematic limit. However, towards lower masses we observe a weaker sensitivity than reported. We note that the discrepancy is well within the bounds coming from input uncertainties as presented for the curve based on empirical inputs.

5 Results

5.1 Impact on Feebly Interacting Particle sensitivities

Combining all the items covered in section 3 (and also appendix B), we have a plethora of different parameters to play with when describing heavy meson distributions at beam-dump experiments. As several Feebly Interacting Particles could be produced in the decays of these heavy mesons, the choice of input parameters has a direct impact on the expected sensitivity of a given experiment to these FIPs. Here, we would like to give a brief idea on the impact this choice has on the resulting sensitivity. For this, we compare the sensitivity of the CHARM experiment [97, 98] to a muonphilic HNL. The experiment had received data corresponding to 2.4×10^{18} dumped protons, the interaction products of which were analysed by a detector array ca. 480m downstream from the CERN WA beam-dump (see appendix E.3 for further details). It was mostly sensitive to HNLs produced in open charmed meson decays, making it an ideal candidate for an isolated impact study of charmed meson distributions.

To evaluate the sensitivity, and consequently the parameter space excluded by the absence of a signal, we use the ALPINIST framework (see section 4). We compare different meson distributions generated with PYTHIA namely

- i. PYTHIA 8.309 in standard settings (`hardQCD:hardccbar`),
- ii. a statistical combination of tables generated with PYTHIA 8.3’s `hardQCD:hardccbar` and `hardQCD:3parton` (c.f. text around figure 18),
- iii. the distributions from the cascade production simulation by the SHiP collaboration [51].

These are contrasted by results using the empirical distribution given in eq. (3.1) with parametrisations as proposed by the CHARM collaboration¹¹ and distributions measured by the LEBC-EHS collaboration [66] (see table 5). These differential cross sections are normalised to match the respective production rates $\chi_{pp \rightarrow c\bar{c}} = \sigma_{c\bar{c}} \sigma_{pp}^{-1}$. To account for the averaged proton-nucleon cross section we apply an enhancement of $A_{\text{Cu}}^{1/3}$ [34, 99]. For

¹¹Note that this parametrisation ($n = 5, a = 2, b = 0$) differs from the dedicated analysis conducted later [81] (see table 2), but was quoted as the underlying distribution for the final HNL search [97].

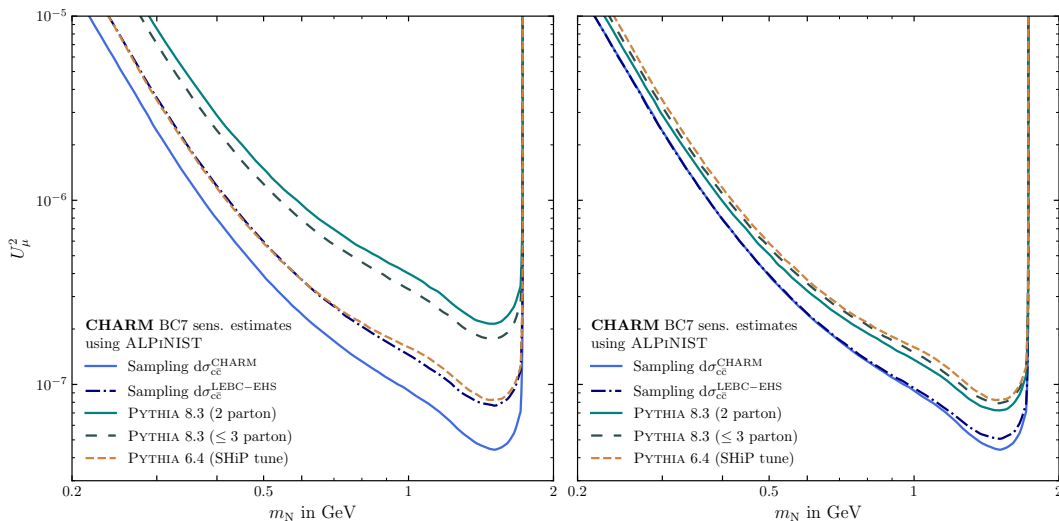


Figure 8. CHARM experiment sensitivity (90% CL excl. bound) to a muonphilic HNL evaluated for different charmed meson distribution inputs. The case of employing the respective production rates associated with the distribution (left) is compared to the case of a common normalised production rate (right). For further information see text.

standard PYTHIA 8.3 this is $\chi_{pp \rightarrow c\bar{c}}^{2 \rightarrow 2} = 4.0 \times 10^{-4}$ which increases to $\chi_{pp \rightarrow c\bar{c}}^{2 \rightarrow 2,3} = 7.2 \times 10^{-4}$ when combining it with `hardQCD:3parton` production. Even though the SHiP cascade production is also based on PYTHIA, we use the commonly referenced value of $\chi_{pp \rightarrow c\bar{c}}^{\text{SHiP}} = 4 \times 10^{-3}$ [39, 50]. We previously found that the flux of neutrinos at the CERN WA beam-dump was consistent with $\chi_{pp \rightarrow c\bar{c}} = 3.5 \times 10^{-3}$ (see section 4.3.1). As the original CHARM search gives no numerical value for the charm production cross section or rate [97], we will adopt this value as the $\chi_{pp \rightarrow c\bar{c}}^{\text{CHARM}}$ rate. For the LEBC-EHS distributions, we have $\chi_{pp \rightarrow c\bar{c}}^{\text{LEBC-EHS}} = 1.5 \times 10^{-3}$ [66, 100].

The resulting sensitivity estimates for a muonphilic HNL at the CHARM experiment are shown in figure 8. The left panel shows the results for meson spectra generated as described above, while the right tile shows the results of a normalised production rate of charmed mesons of $\chi_{pp \rightarrow c\bar{c}} = 3.5 \times 10^{-3}$ for all spectra. Including the differences in integrated cross section $\sigma_{c\bar{c}}$ (figure 8 left), we observe differences in the expected sensitivity up almost an order of magnitude. The differences due to production cross section are a constant factor (with respect to m_N) between the sensitivity curves. When normalising $\chi_{pp \rightarrow c\bar{c}}$ (figure 8 right), the differences between curves represent only the impact of the underlying D meson kinematics.¹² For $m_N < 0.5$ GeV, the difference between the curves is of the order of 2. When approaching the kinematic limit, the gap between PYTHIA generated mesons and sampled from empirical distributions widens reaching a maximum of around a factor of 4. This shows, that while the integrated production cross section has an obvious impact on the sensitivity estimate, the substantial contribution of the associated kinematic distributions

¹²The maximum difference between the fragmentation functions was $\sim 17\%$, resulting in a subleading difference in sensitivity of $\sim 8\%$.

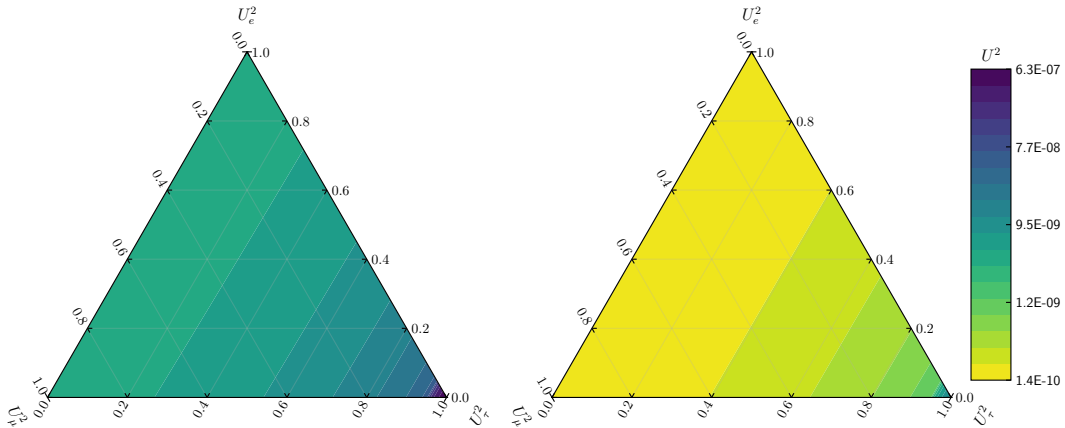


Figure 9. The DUNE-ND (left) and SHiP (right) predicted HNL sensitivities (90% CL excl. lower bound) for different coupling combinations assuming $m_N = 1.5$ GeV and charmed meson distributions as given by PYTHIA 8.3.

must not be overlooked.

5.2 Beyond benchmark cases

A common way to present HNL sensitivities without having to resort to benchmark case scenarios is the ternary representation at a fixed mass. The three axes grid indicates ratios between the individual leptonic couplings U_α^2 , while the maximal sensitivity to $U^2 = U_e^2 + U_\mu^2 + U_\tau^2$ can be shown in colour scale. Figure 9 shows the expected U^2 90% CL lower bound sensitivity limit for the future DUNE Near Detector [101, 102] and SHiP [8] experiments in such a representation for an HNL with mass $m_N = 1.5$ GeV, with logarithmic colour scale. The predicted sensitivities for both experiments follow a similar pattern, where in the case of coupling to light leptons (e and μ along the top left axis) the sensitivity is roughly similar, while it strongly decreases as the τ coupling component becomes more dominant (bottom right corner).

This representation also allows us to investigate the impact of meson distribution choice for different coupling combinations. For this, we calculate expected sensitivities based on the fit result central values for the parametrisation of the differential meson production cross section described by eq. (3.1) found in section 3.2. Consequently, we normalise the resulting expected sensitivity to the values found by using PYTHIA 8.3 to generate the meson distributions shown in figure 9. The resulting sensitivity ratios are presented in figure 10 for the proposed DUNE-ND and SHiP experiments. Both experiments are expected to be more sensitive when considering the empirical meson production cross sections. We attribute this to the fact that PYTHIA estimates harder p_T meson spectra than observed in data (c.f. figure 3 right) leading to more HNLs going out of acceptance. This effect is less pronounced in the baseline SHiP case, as the large angular coverage means that few HNLs go out of acceptance even in the PYTHIA case. This effect is especially pronounced in

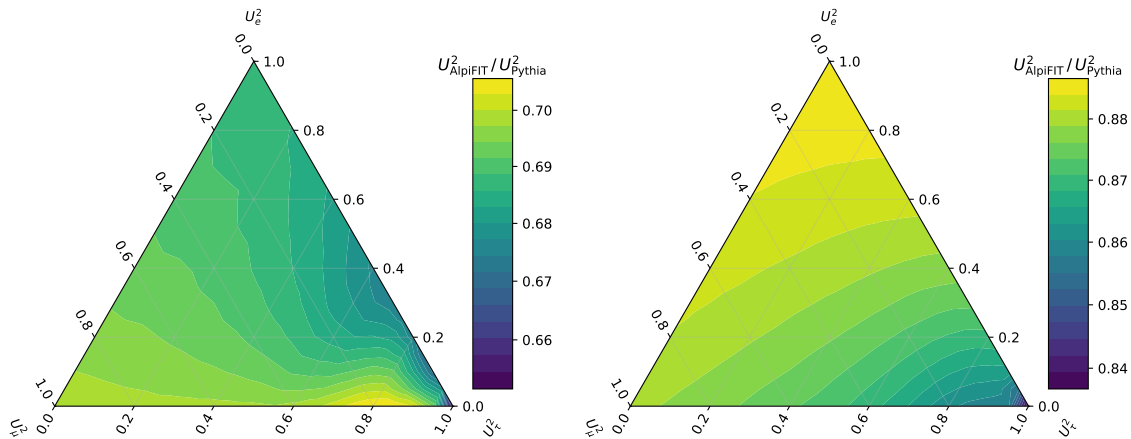


Figure 10. Impact on the underlying meson distribution choice on the DUNE-ND (left) and SHiP (right) predicted HNL sensitivities (90 % CL excl. lower bound) for different coupling combinations assuming $m_N = 1.5$ GeV. The sensitivity calculated with meson distributions as given by the central fit values of the parametrisation presented in section 3.2 is normalised to the sensitivity based on PYPHIA 8.3 inputs shown in figure 9.

the τ -philic case, as the production through intermediate τ leptons exacerbate this effect. Furthermore, it is important to note that the standard deviation in $1 - U_{\text{AlpiFIT}}^2 / U_{\text{Pythia}}^2$ is of the order of few to several percent with respect to the mean for both experiments.¹³ Therefore, the impact of the meson spectra on the expected sensitivity can be viewed to first order as a coupling independent effect. This is especially true in the regime where τ coupling is minimal, as here kinematically similar channels dominate in the mass regimes relevant to beam-dump searches.

5.3 Impact on the sensitivity landscape

As the example case presented in section 5.1 shows, the choice of heavy meson (differential) production cross sections greatly impacts the sensitivity expectation of beam-dump style experiments to HNLs. In the absence of perfectly perfectly reliable experimental data for these cross sections, a comparison between experiments with the same underlying biases is warranted. ALPINIST is uniquely suited for this task as it

- i. reliably reproduces existing experimental bounds (see section 4.3),
- ii. easily adapts underlying meson distributions,
- iii. analyses the different experiments in the same underlying theory framework.

In this section we present the collective past exclusions, current parameter reaches and future projected sensitivities to the most commonly considered HNL benchmark cases (BC6: e -philic, BC7: μ -philic, BC8: τ -philic) of beam-dump-style experiments derived under the assumptions established in this work. For this, we compare the past BEBC [95], CHARM [97], NuTeV [92], the ongoing NA62 [103, 104] in beam-dump mode (NA62-bd)

¹³Indeed, this is the case for all experiments presented in this work.

and DarkQuest Phase-I [105], and future DarkQuest Phase-II [105], DUNE near detector [101, 102], and SHiP [8] experiments.

Figures 11 and 12 show such comparisons of the above experiments for different meson input assumptions. These figures show

- parameter space which is presently excluded by light meson decay precision experiments [106–113] and collider based experiments [114–118] as grey shaded regions,
- parameter exclusion coming from beam-dump searches for HNLs [87, 92, 97] as light grey shaded regions,
- ALPiNIST recasts of these concluded beam-dump experiment searches with no significant signal events (i.e. already excluded parameter space within the experimental sensitivity) as solid lines,
- ALPiNIST expectations for sensitivities of running experiments as dashed lines,
- ALPiNIST sensitivity predictions for future experiments based on the respective baseline scenarios represented as dotted lines.

We present all curves as the 90% CL exclusion limits, which for most experiments corresponds to an expected number of $n_{90\% \text{ CL}} = 2.3$ events (i.e. background free assumption). The exception to this are the DarkQuest and DUNE experiments which estimate $n_{90\% \text{ CL}} = 10$ [101, 105], and BEBC in the BC7 case where $n_{90\% \text{ CL}} = 3.45$ due to observed events [95]. The shaded regions surrounding the curves of the same colour correspond to a variation of input assumptions within 68% CL limits as described below.

Figure 11 presents these sensitivities with PYTHIA 8.309 in standard settings as a generator for the heavy mesons, while the overall meson production cross sections are the fit results on experimental data taken from section 3.1 (summarised in table 1) without cascade production factors. The uncertainties, represented by bands of the same colour as the lines, correspond to the propagated variation of the production cross sections within the 68% CL fit limits. To the authors’ knowledge, for the first time we show the NuTeV sensitivities in the BC6 and BC8 plots. This is possible as – even though NuTeV was only sensitive to final states containing muons and therefore mostly BC7 – the sensitivity to BC6 and BC8 stems from the final states $\nu\mu\mu$ being available through neutral current interactions, as well as $\nu e\mu$ also being a charged current mediated final state of BC6. For the NuTeV experiment we also note that using the charmed meson production as shown in table 1 lowers the exclusion power in the case of BC7 with respect to the value used in the original search [92], but also relative to the BEBC and CHARM searches. This is also due to, as already shown in recent recasts [50, 96], the parameter exclusion in all mixing scenarios by the BEBC and CHARM experiments being stronger than originally published [95, 97].¹⁴ We find the general hierarchy between the planned future experiments, as well as the order of improvement with respect to present and past experiments to be similar to what is commonly depicted in literature.

¹⁴As we are not able to fully reproduce the published CHARM limits with the assumptions given in the paper (c.f. appendix E.3) the related exclusion limits should be taken with a grain of salt.

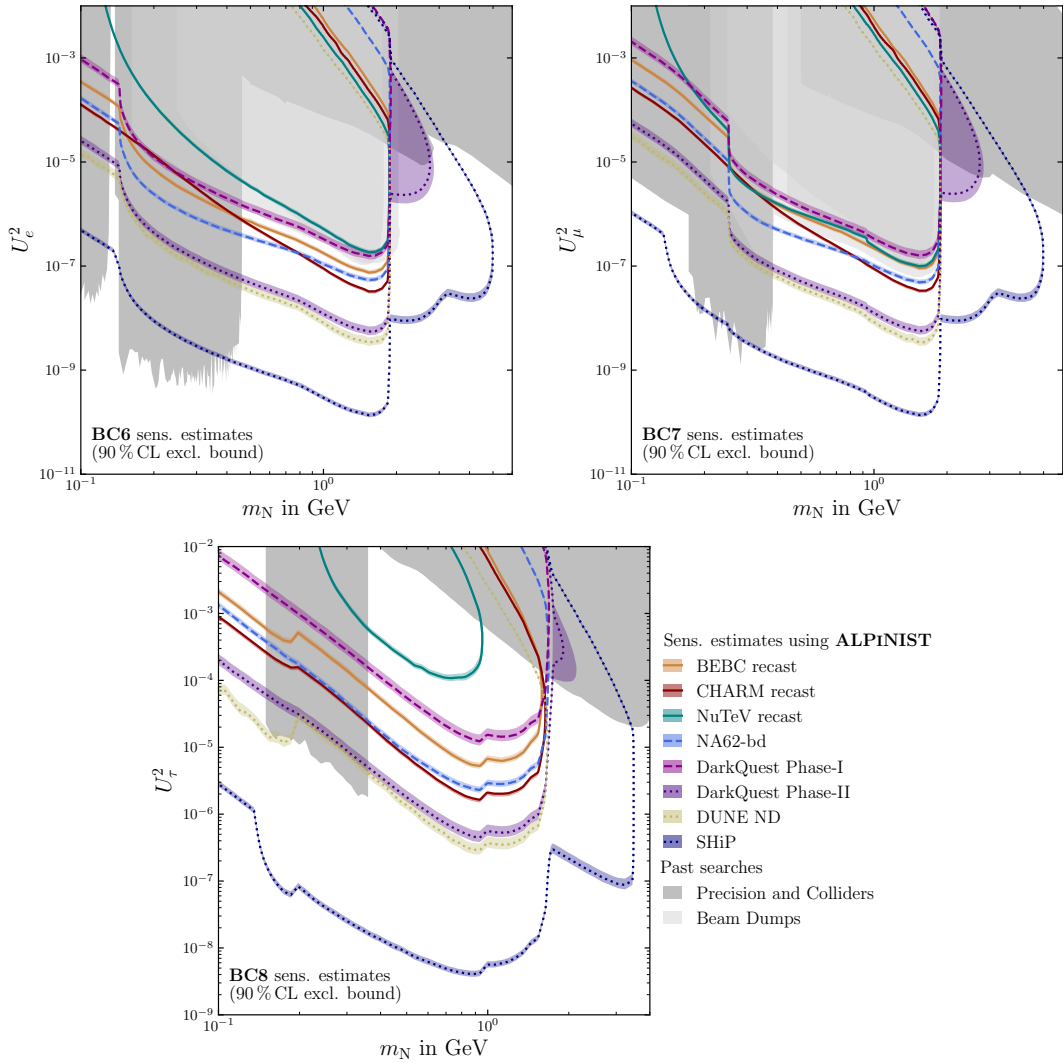


Figure 11. Sensitivities (90% CL excl. bound) of various past (solid lines) present (dashed lines) and future (dotted lines) beam-dump style experiments to Benchmark Case scenario HNLs (electron-philic top left, muon-philic top right, tau-philic bottom). The underlying meson distributions are generated using PYTHIA 8.3, with quark level cross sections $\sigma_{q\bar{q}}$ as given in table 1. The coloured bands surrounding the lines correspond to varying $\sigma_{q\bar{q}}$ s within the 68% CL bounds. The grey shaded area is parameter space excluded by light meson decay precision experiments [106–113], as well as collider based experiments [114–118]. The light grey shaded regions represent the parameter space excluded by beam-dump searches [87, 92, 97]. For further details see text.

Figure 12, on the other hand, shows the same sensitivities with the same cross sections, but with the heavy meson differential distributions sampled from the empirical distribution eq. (3.1) with experimentally motivated parameters as established in section 3.2. The presented uncertainties represent the propagated variation of both the production cross section and the parameters entering eq. (3.1) within the respective fit uncertainties. The multiplicities of the different open meson species per $q\bar{q}$ event are taken from PYTHIA 8.309

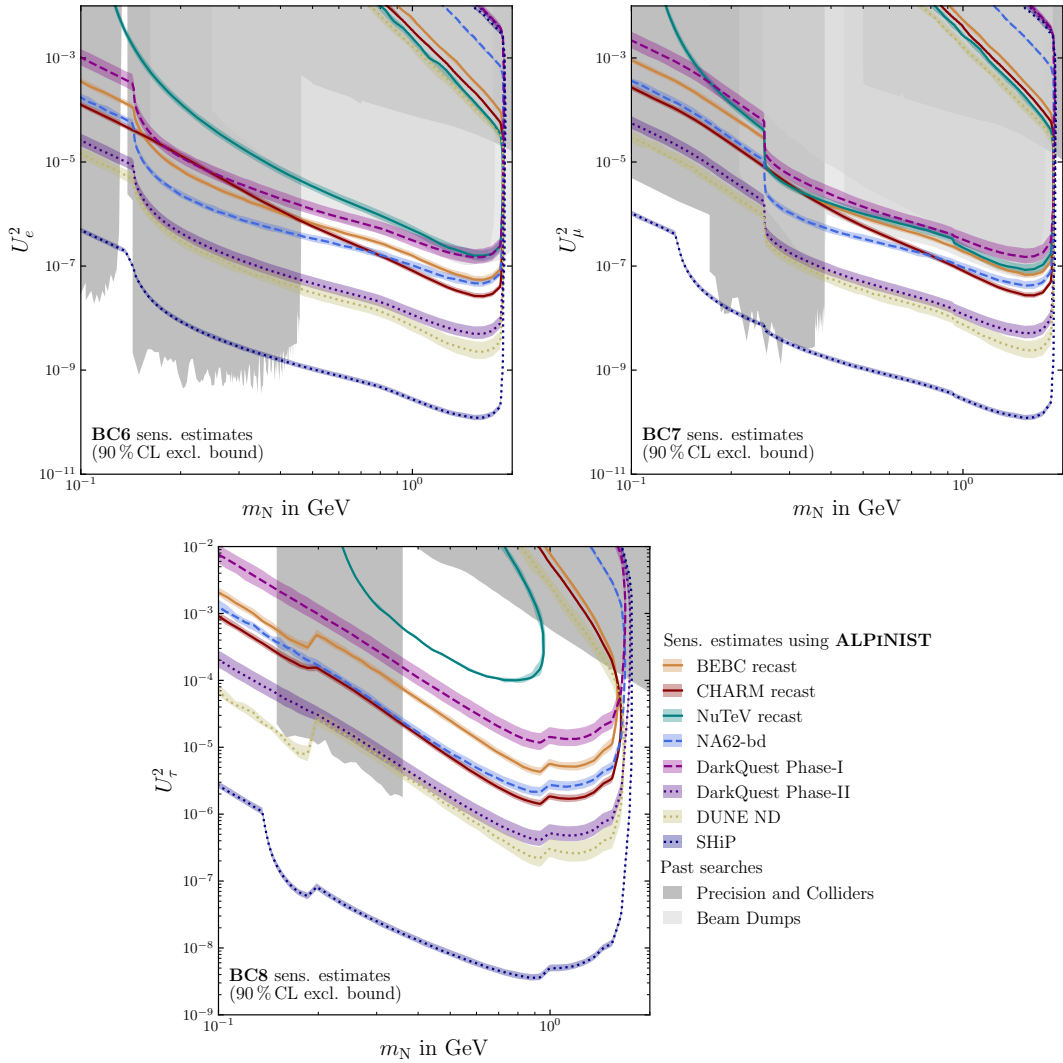


Figure 12. Sensitivities (90% CL excl. bound) of various past (solid lines) present (dashed lines) and future (dotted lines) beam-dump style experiments to Benchmark Case scenario HNLs (electron-philic top left, muon-philic top right, tau-philic bottom). The underlying meson distributions are generated using the parametrisation eq. (3.1) with parameters as given in table 3, and quark level cross sections $\sigma_{c\bar{c}}$ as given in table 1. The coloured bands surrounding the lines correspond to varying $\sigma_{c\bar{c}}$, $b_{c\bar{c}}$, and $n_{c\bar{c}}$ within the 68% CL bounds. The limitation to charmed meson production is due to the lack of experimental beauty meson data. The grey shaded area is parameter space excluded by light meson decay precision experiments [106–113], as well as collider based experiments [114–118]. The light grey shaded regions represent the parameter space excluded by beam-dump searches [87, 92, 97]. For further details see text.

due to a lack of data. Notably, in this procedure, beauty meson contributions to the experimental sensitivities are not included as there is no experimental data available for differential cross sections at the relevant centre-of-mass energies (c.f. section 3.2.2). In the remaining sensitive parameter space, the relative differences between sensitivities are

similar to those in figure 11. Meanwhile, we observe a slight sensitivity improvement on a global scale similar to the values presented in figure 10 shifting the lower bounds by factors around ~ 0.8 .

6 Conclusions

Heavy Neutral Leptons are an excellently motivated candidate for BSM physics that address a number of shortcomings in the Standard Model. The search for them is thus highly motivated and a number of proposals have been put forward and are poised to scan significant portions of the HNL parameter space [6, 8, 101, 119]. A promising way to find or exclude HNLs are proton beam-dumps. In these configurations, HNLs are typically produced from decays of heavy mesons produced in the forward direction of the proton interaction. However, there is little experimental data available, for heavy meson production in this kinematic range. For a credible search program, especially for those with data already on tape [93, 103, 104], it is thus mandatory to study possible differences in existing data and MCs typically employed for projected sensitivities.

In this paper we have systematically studied the impact viable assumptions on meson distributions can have on the predicted sensitivity of an experiment. To this effect, we have identified the underlying meson production parameters and attempted to collect the available experimental data in a unified set-up. We have used the updated implementation of the ALP_{INIST} code to simulate HNLs from their production up to the detector response to the decay products in a simplified MC framework. Varying the meson inputs within motivated assumptions, we demonstrated that the experimental sensitivity can shift by up to an order of magnitude in the coupling suppression. This effect was shown to be largely independent of the HNL coupling structure to the standard model. Finally, for the first time, we have compared the sensitivities of different beam-dump experiments on equal footing both in terms input and also model parameters, albeit in a simplified MC set-up.

This work also highlights the need for further experimental constraints on the heavy meson spectra in proton nucleus interactions. We would like to emphasise that ongoing experiments like DsTau [120] and SHiP-charm [35] at CERN may already take a large step towards a better understanding of the charm production. However, especially for beauty mesons, where experimental input is virtually non-existent, experimental validation of theory based simulations is needed. On the theory side, implementations of heavy quark generation mechanisms beyond $gg \rightarrow q\bar{q}$ and $q'\bar{q}' \rightarrow q\bar{q}$ in simulation frameworks like PYTHIA will likely be helpful in describing the meson spectra more accurately. Steps toward this have already been taken (c.f. appendix B).

Another important point to raise is that HNLs are special among the commonly considered FIPs in that they are produced in large numbers in open charmed decays. For other FIPs like Axion-Like-Particles and Dark Photons, especially the beauty mesons are relevant in some production scenarios [1]. Yet, for these FIPs other channels like dark bremsstrahlung and mixing dominate, making accurate B -production prescriptions a secondary matter to

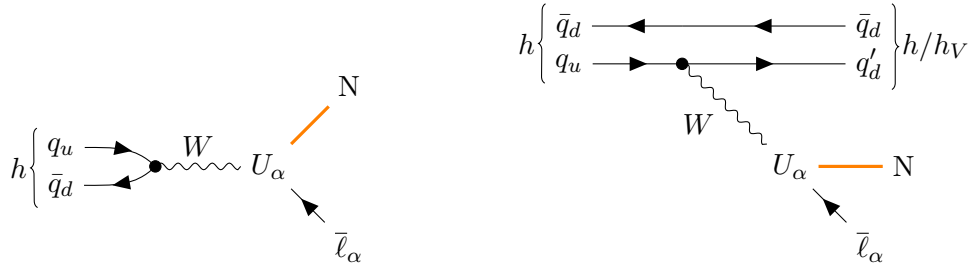


Figure 13. Dominant HNL production channels in the $\mathcal{O}(100 \text{ MeV to } 1000 \text{ MeV})$ mass regime. In case the HNL is a Majorana particle, the charge conjugated process is allowed.

inconsistencies in the commonly used radiation approximations [121] and mixing formalism [122]. In the case of the Dark Scalar, however, beauty meson decays are a dominant production mechanism [1], highlighting again the relevance of accurate beauty meson spectra. In summary, especially beam-dump experiments that hope to exploit beauty meson decays to search for Feebly Interacting Particles should be very interested in exploring the relevant meson spectra from an experimental side.

Acknowledgements

We would like to thank I. Abt and T. Hebbeker for discussions on the CHARM HNL limits and to M. U. Ashraf for discussions on the Pythia tunes. In addition, we gratefully acknowledge discussions with M. Ovchinnikov on the heavy meson spectra and FIP phenomenology. The authors acknowledge very useful conversations within the NA62 experiment. This study is performed independently of any experiment. This work is supported by the European Research Council under grant ERC-2018-StG-802836 (AxScale project). We also acknowledge discussions within COSMIC WISPerS CA21106, supported by COST (European Cooperation in Science and Technology).

A Heavy Neutral Lepton interactions

As already highlighted in section 2.2, the HNL is produced and decays in U -suppressed weak interactions. The relevant width-formulae are well established [43, 47, 48]. In case of minor discord in the literature, we rely on the calculations by Bodarenko et al. [43]. As their review is very exhaustive, we would like to point the interested reader there. In the following we will only give a very brief summary, focusing on the points where our implementation diverges.

A.1 Production

The main production channels for HNLs in the $\mathcal{O}(100 \text{ MeV to } 1000 \text{ MeV})$ range are the two and three-body decays of pseudoscalar mesons as sketched in figure 13. In particular,

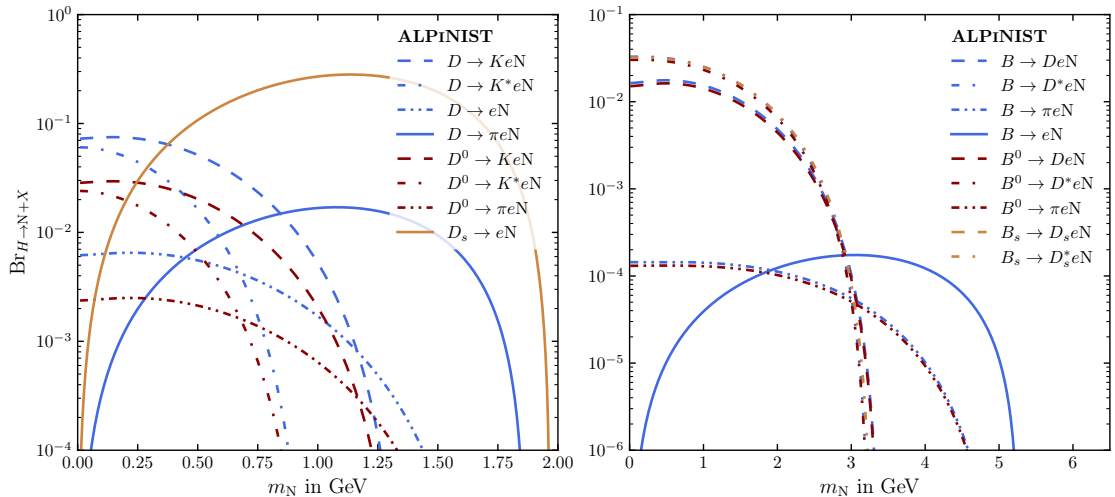


Figure 14. Branching ratios of open charm (left) and beauty (right) mesons to an electronphilic HNL N with coupling U_e^2 normalised to 1.

the decays of open charmed and beauty mesons are relevant for the production at energies typical for beam-dump experiments [43]. The bulk of HNLs are produced in their (semi-) leptonic decays with up to a single pseudoscalar or vector meson in the final state.¹⁵ This corresponds to signatures such as $h_P \rightarrow \ell N$, $h_P \rightarrow h'_P \ell N$, and $h_P \rightarrow h_V \ell N$, where we focus on the dominant contributions with $h_P \in (\pi, K, D)$ and $h_V \in (K^*, D_s^*)$.

For two-body decays of the $h_P \rightarrow \ell N$ type, the relevant pseudoscalar decay constants have been taken from PDG22 and where necessary FLAG21 review tables [79, 123]. For three-body decays the underlying tabulated values are taken from the structure functions, where N is replaced with the SM neutrino. The underlying parameters have been updated to match best fit values presented in the FLAG21 review [123] for pseudoscalar meson decays into other pseudoscalars ($h_P \rightarrow h'_P \ell N$), while the decays into vector mesons have been matched to best fit results by the HPQCD collaboration [124, 125] for the decay of beauty mesons ($B \rightarrow h_V \ell N$). For the decay $D \rightarrow K^* \ell N$ we follow Bondarenko et al. [43] using the form factors listed by Melikhov and Stech [126]. The resulting branching ratios for production in open charmed and beauty meson decays considered in the `EXO_decay` module of ALPiNIST are presented in figure 14 for a coupling ratio $(U_e^2 : U_\mu^2 : U_\tau^2) = (1 : 0 : 0)$.

We finally note, that HNLs can also be produced in the decays of light pseudoscalar mesons [43]. However, unlike for the mixing other FIPs undergo, the reabsorption rate of mesons and the propagation distance from the primary interaction point at decay time is strongly modulated by the composition and geometry of an experiments specific dump (K_S being a borderline case). In the spirit of generalisability, we leave the simulation of these effects to experiments' dedicated full MC set-ups. We would like to further point

¹⁵In the massless HNL limit, where the neglected contributions are maximal, they make up around 20% of the total possible yield.

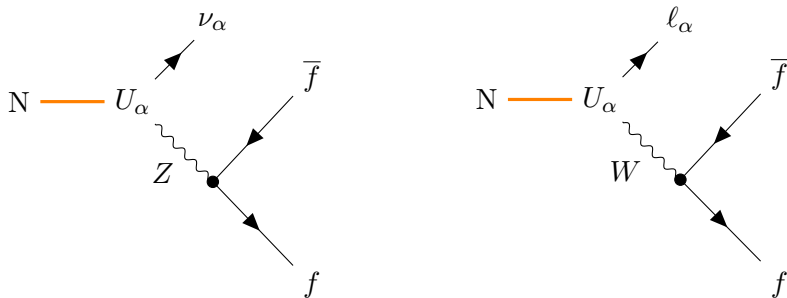


Figure 15. Leading order HNL decay channels in the $\mathcal{O}(100 \text{ MeV to } 1000 \text{ MeV})$ mass regime. In case the HNL is a Majorana particle, the charge conjugated process is allowed.

out, that light meson precision experiments routinely surpass beam-dumps in terms of sensitivity in this mass regime due to favourable scaling in terms of coupling suppression (c.f. figures 11 and 12).

A.2 Decay

The HNL with a coupling as described by eq. (2.3) most commonly decays into three fermions as schematically presented in figure 15. In the Z -mediated case, f can either represent a lepton or a quark, while in the W -mediated case $f'\bar{f}$ is either a neutrino anti-lepton pair or a up- anti-down-like pair of quarks. The leptonic decay channels of the HNL depend on the exact ratio of its mixing angles, but are of the structure $\nu\ell\bar{\ell}^{(\prime)}$ with $\ell = e, \mu, \tau$ and also include the invisible 3ν final state. The most relevant hadronic decay channels are of the kind lh_P, lh_V for charged pseudoscalar (vector) mesons $h_P (h_V)$ and their neutral counterparts $\nu h_P, \nu h_V$. Of particular note are the decays to $\ell\pi$ and $\ell\rho$ as they leave a clear signature in a detector. However, for the relevant calculations we also include the above combinations with $h_P \in (K, \eta, \eta', D, D_s, J/\psi)$ and $h_V \in (\rho, \omega, \phi, D_s^*)$.

In case of a semileptonic decay, the QCD interactions of the produced quarks play a major role in the width of the HNL. In case the quarks form a stable meson, the decay can be well approximated as a two-body decay including the appropriate form factors. However, for HNLs heavier than twice the pion mass, also multibody bound QCD final states become possible. This is of particular importance when calculating the total width of the HNL. Following Bodarenko et al. [43], we estimate their importance using the hadronic width ratio of the τ lepton $R_{\tau,h} = \Gamma(\nu_\tau + \text{had})\Gamma^{-1}(\nu_\tau + e\bar{\nu}_e)$, which is known up to N⁴LO in $\alpha_S(m_\tau)\pi^{-1}$ [127, 128]. We then promote $R_{\tau,h}$ to relate the approximated full hadronic width of the HNL to its charged and neutral current decays with u and/or d quarks in the

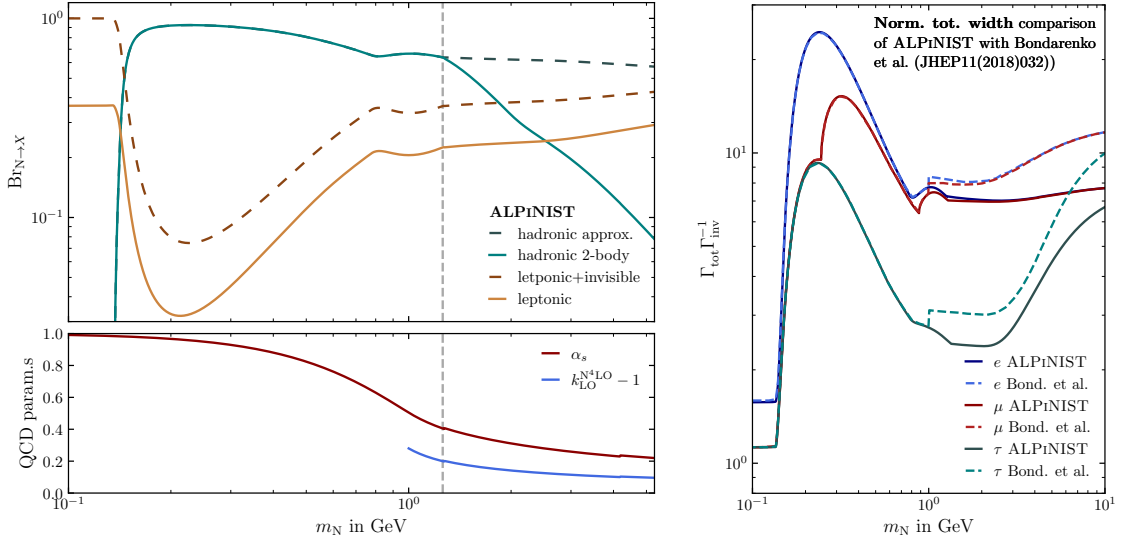


Figure 16. Left: Branching ratios of hadronic and leptonic decay channels of an electrophilic HNL (top), with solid lines indicating the observable components and dashed lines the contributions to the total width. Underlying QCD related parameters strong coupling α_s and scaling ratio $k_{LO}^{N^4LO}$ (bottom). Right: Comparison of total decay widths normalised to the decay width to invisible (3ν final state) for the different coupling dominance scenarios (e -BC6, μ -BC7, and τ -BC8) between the implementation in ALPiNIST and Bondarenko et al. [43]. For further information see text.

final state with $\alpha_S = \alpha_S(m_N)$ as¹⁶

$$k_{LO}^{N^4LO} = 1.019 \left(0.994 + \frac{\alpha_S}{\pi} + 1.640 \left(\frac{\alpha_S}{\pi} \right)^2 + 6.371 \left(\frac{\alpha_S}{\pi} \right)^3 + 49.076 \left(\frac{\alpha_S}{\pi} \right)^4 \right). \quad (\text{A.1})$$

Using the β evolution for the running of the strong coupling [128] up to β_3 , and connecting it below $q < 1$ GeV with a third order polynomial ensuring that $\alpha_s(q)$ run smoothly to $\alpha_s(q = 0) = 1$, we get an approximation ratio as shown in the bottom left panel of figure 16.

For HNL masses above 1 GeV we then calculate the semileptonic HNL width as the maximum between the thus calculated approximate width and the possible two-body semileptonic decays considered. This ensures, that $\alpha_s \pi^{-1}$ is already in a perturbative regime justifying the $R_{\tau,h}$ approach. The resulting branching ratios for (visible) leptonic and (approximated) hadronic decays of an electrophilic HNL are shown in the top left panel of figure 16. Typically, the semileptonic width is then approximated for masses just above the 1 GeV threshold, as indicated for this case by the grey dashed line. Notably, this results in a total HNL width that differs from the prescription by Bondarenko et al. [43] in all benchmark cases for HNL masses above 1 GeV (see figure 16 right).

¹⁶This formulation is the N^4LO approximation of $R_{\tau,h}$ in \overline{MS} at $\alpha_s = \alpha_S(m_\tau)$ [127, 128], not including the number of quark colours and CKM suppression, as these are included in the reference widths.

B Leading particle effects on meson distributions

The leading particle effect describes an asymmetry in hadron collisions, where the x_F and p_T spectra of secondary particles sharing a valence quark with the beam particle are harder with respect to their charge conjugate partners that do not have such a valence quark in common. From the theory side, many ideas have been put forward to derive this experimentally observed asymmetry ranging from intrinsic charm coalescence [129, 130], charm excitation [131], over-production in colour strings (used in the standard configuration of PYTHIA) [132–134], to heavy recombination [135] and light fragmentation [136]. In all these models, any asymmetry in the hard x_F region of open charm/beauty meson production can be attributed to the valence quarks of the beam particle either as remnants involved in the recombination or as initial states to the scattering process. In the following we will give some insight in the experimental validation of these ideas at beam-dump energies.

B.1 Open charmed mesons

Leading particle effects were observed experimentally in the differential spectra of open charmed mesons in $\pi^- N_{C/Ti}$ [137] as well as $\Sigma^- N_{Be}$ scattering [138]. However, in 400 GeV protons scattering on N_{H_2} , the LEBC-EHS collaboration (NA27) observed an asymmetry preferring hard D^+ and D^0 mesons over their charge conjugate partners in the high x_F regime [66]. A comparison of these results with PYTHIA 8.3 is shown in figure 17, where both the differential cross sections from PYTHIA ($k_{c\bar{c}} = 1$) and that scaled to match the cross section found by LEBC-EHS ($k_{c\bar{c}} = 3.7$) are shown. A tension between expected and measured values is present. Data from pN_{Cu} scattering by the WA82 experiment [64] at a similar beam energy of 370 GeV is in better agreement with theoretical models.¹⁷ We would like to highlight that the intrinsic charm model, further substantiated by the recent findings using LHCb data [142, 143], could lead to asymmetries specific to pN scattering that would not occur in $\pi^\pm N$. It is, however, beyond the scope of this work to establish a new theoretical framework for describing the production mechanisms of open charmed mesons. Therefore, we limited ourselves to using the LEBC-EHS and other measured differential cross sections as inputs for a subsequent FIP simulation.

In recent versions of PYTHIA 8 a new option for simulating HardQCD processes was added, namely the `HardQCD:3parton` functionality. This allows the simulation including $2 \rightarrow 3$ diagrams describing parton level scattering. In principle, this introduces production channels of open charmed mesons, where a charmed quark can combine with a parton involved in the scattering process, as required by heavy recombination [135]. This is in contrast to the standard colour string scheme of PYTHIA, where the combination only occurs with

¹⁷As presented in table 5, the tension is somewhat less significant in our reevaluation of the spectral data for the case of D^\pm , however still persists for \bar{D}_0 .

Employing a different PYTHIA reconnection scheme based on QCD colour of the beam remnants [139] results in overall harder x_F meson spectra while the p_T spectra are softer, which also releases the tension. However, we still observe a major discrepancy in the p_T spectra.

We found the Ropewalk mechanism [140, 141] to have little impact on the resulting spectra.

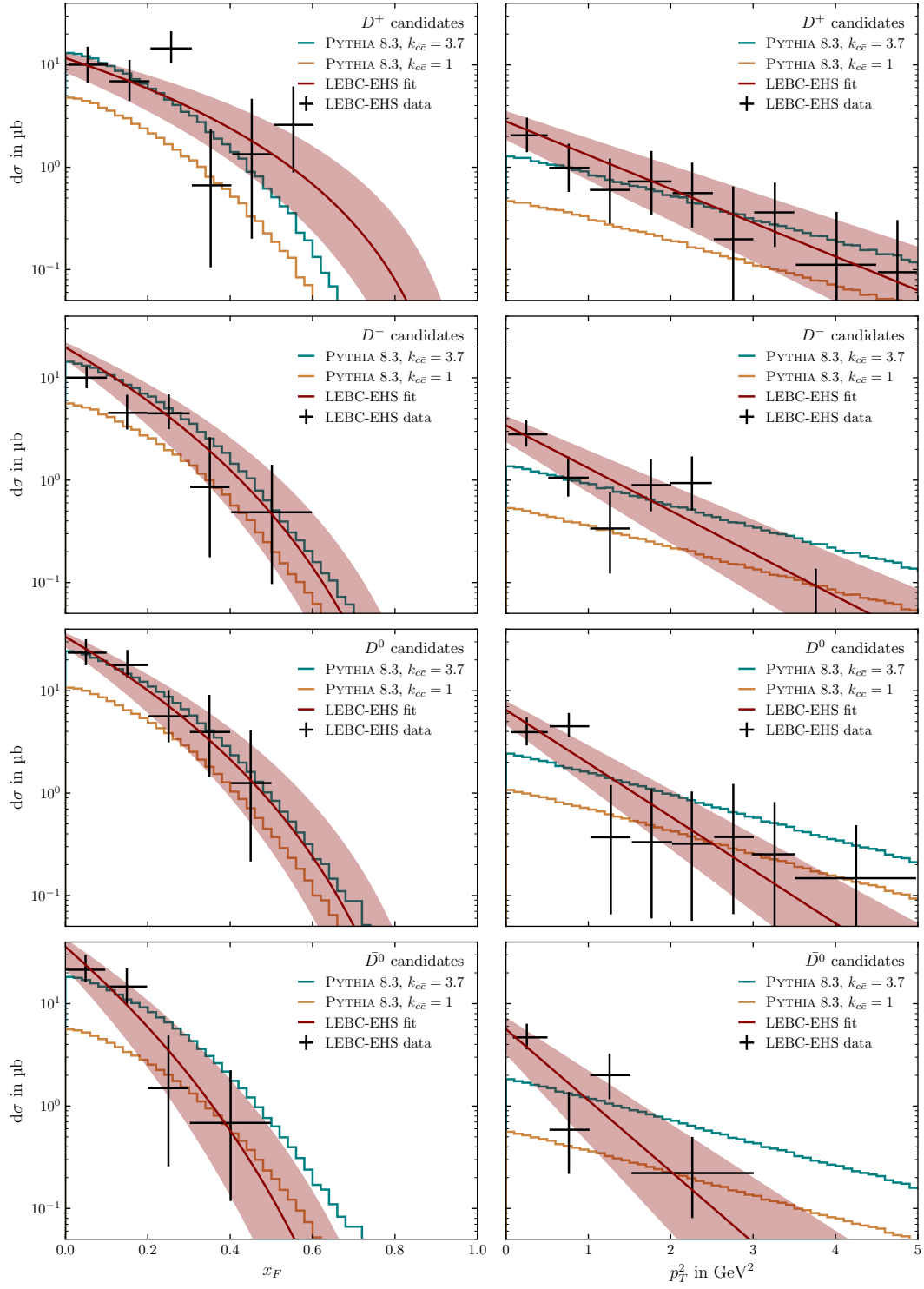


Figure 17. Comparison of x_F and p_T^2 spectra for different open charmed mesons as measured by the LEBC-EHS collaboration [66] compared to results from PYTHIA 8.3 with PYTHIA suggested ($k_{c\bar{c}} = 1$, orange) and adjusted ($k_{c\bar{c}} = 3.7$, teal) cross section $\sigma_{c\bar{c}}$.

beam remnant parts. However, as of the writing of this paper, the `HardQCD:3parton` processes are only implemented with amplitudes assuming massless quarks. This is especially concerning, as these processes can scale explicitly with the quark mass [135]. We verified that in the standard PYTHIA production of open charmed meson production in $2 \rightarrow 2$ processes, no significant difference in x_F or p_T spectra was observed between considering the charmed quark massive or massless. Even though the extension of this check to $2 \rightarrow 3$ processes is far from sound, we present in figure 18 the impact on the spectra of charmed and anti-charmed quarks when considering the three-parton processes and weighting the contributions between two- and three-parton processes with the associated cross section estimated by PYTHIA. The x_F spectra for open anti-charmed mesons (upper left) are roughly comparable when considering only $2 \rightarrow 2$ compared to $2 \rightarrow 2, 3$ processes, while the open charmed meson x_F spectra (bottom left) are slightly softer when also considering $2 \rightarrow 3$. The p_T spectra are significantly harder for all mesons when including the $2 \rightarrow 3$ processes. This is in worse agreement with experimental data (c.f. figure 3).

	LEBC-EHS		Refits	
	n	b	n	b
D^+	3.1 ± 0.8	0.75 ± 0.14	4.94 ± 2.54	0.67 ± 0.09
D^-	5.4 ± 1.2	0.93 ± 0.18	5.1 ± 1.07	1.24 ± 0.43
D^0	5.4 ± 1.1	1.04 ± 0.19	5.47 ± 0.8	1.97 ± 0.68
\bar{D}^0	8.1 ± 1.9	1.49 ± 0.32	9.25 ± 2.84	1.87 ± 1.04

Table 5. LEBC-EHS parametrisations of individual open charmed mesons [66] for differential production cross sections as given by eq. (3.1). Also presented are the results of refits performed on the published LEBC-EHS data points, assuming the presented uncertainties as standard deviations in a orthogonal distance reduction fit.

B.2 Open beauty mesons

In principle, one would expect the leading particle effect to also impact the spectra of beauty mesons. However, given the lack of experimental data we limit ourselves here purely to analysing the impacts with PYTHIA. Figure 19 shows the B meson differential distribution, using PYTHIA’s `HardQCD:3parton` with `HardQCD:nQuarkNew=5`. The spectra for anti-beauty mesons generated with only $2 \rightarrow 2$ processes do not show sizeable differences to those generated including also $2 \rightarrow 3$ parton-level processes. For beauty mesons, the x_F spectra for the B^+ and B^0 are significantly harder when also including $2 \rightarrow 3$ parton level processes, while the corresponding B_s spectrum does not change significantly. In all cases, the p_T spectra show little discrepancy between the two approaches. We observe, however, that comparing the $2 \rightarrow 2$ process `HardQCD:hardbbbar` using a massive b quark and the massless equivalent of `HardQCD:qqbar2qqbarNew` combined with `HardQCD:gg2qqbar` and `HardQCD:nQuarkNew=5`, the spectra differ significantly. Moreover, the transverse effects due to $2 \rightarrow 3$ diagrams scale with the quark mass [135]. Therefore, it is questionable whether the $2 \rightarrow 2, 3$ spectra shown in figure 19 paint a more accurate picture than those of only the $2 \rightarrow 2$ processes.

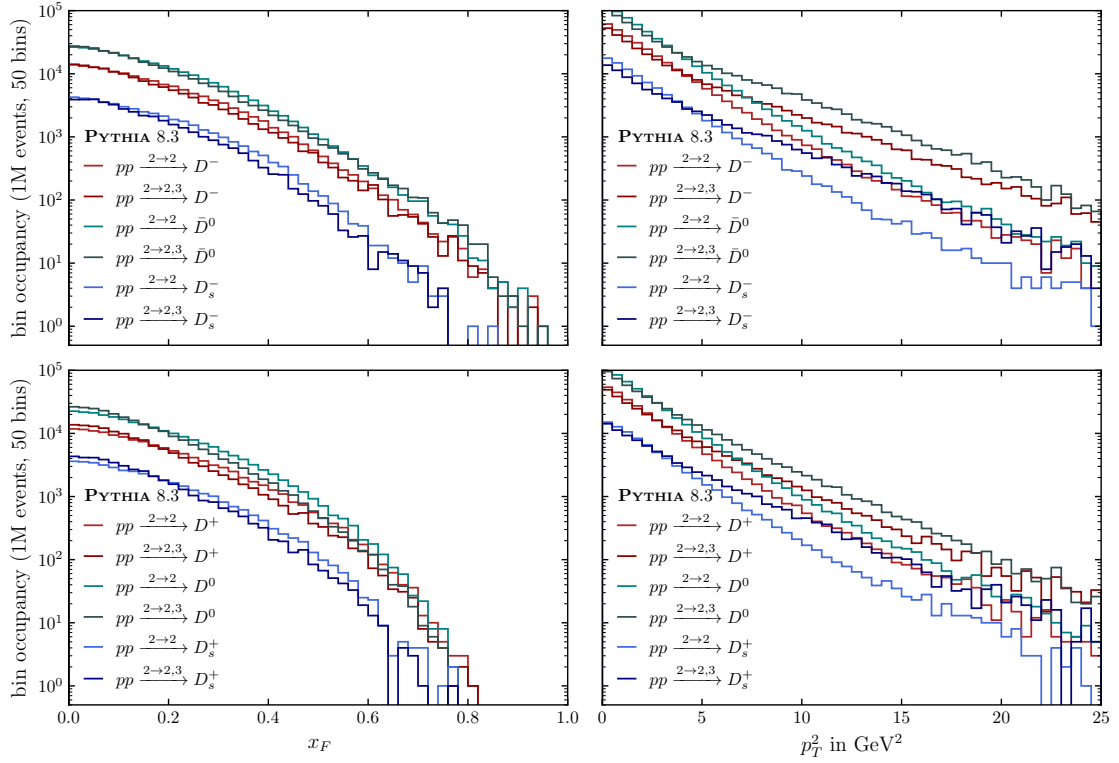


Figure 18. Comparison of x_F and p_T^2 spectra considering PYTHIA’s `HardQCD:hardccbar` ($2 \rightarrow 2$) and a weighted combination including `HardQCD:3parton` with `HardQCD:nQuarkNew=4` ($2 \rightarrow 2, 3$) for open charm and anti charm mesons in the top and bottom panels respectively in $\sqrt{s} = 27.43$ GeV pp scattering.

C Fit details

The underlying framework for all the fits presented in section 3 is the PyMC Gaussian Process [60] which we use to perform a Bayesian fit to the data. The heart of the fit is the Matérn covariance function with $\nu = 5/2$ as the Gaussian Process’ kernel function. To this we assign a gamma distributed length scale with variable α_{ls} and β_{ls} scales, and a half normally distributed amplitude with variable scale σ_{amp} . The models are assumed normally distributed at a given x (\sqrt{s}) using a theory motivated prior with expectation value μ_{prior} and standard deviation σ_{prior} . The posterior distribution is then generated by marginal likelihood minimisation at new x values (120 points from $x_{\text{min}}^{\text{new}}$ to $x_{\text{max}}^{\text{new}}$). The (initial) values used for the specific fits are summarised in table 6. This choice of covariance function and model building is motivated by its ability to fit data points with a cohesive function, while the uncertainty is modulated by the data point uncertainties, data point multiplicities, and the notion of x distance to data. The initial values for the covariance function were then derived by a parameter scan with the goal of allowing a dynamic enough x -dependence to match the data in terms of overall likelihood optimisation, while avoiding divergences and strong oscillations (overfitting) on qualitative grounds.

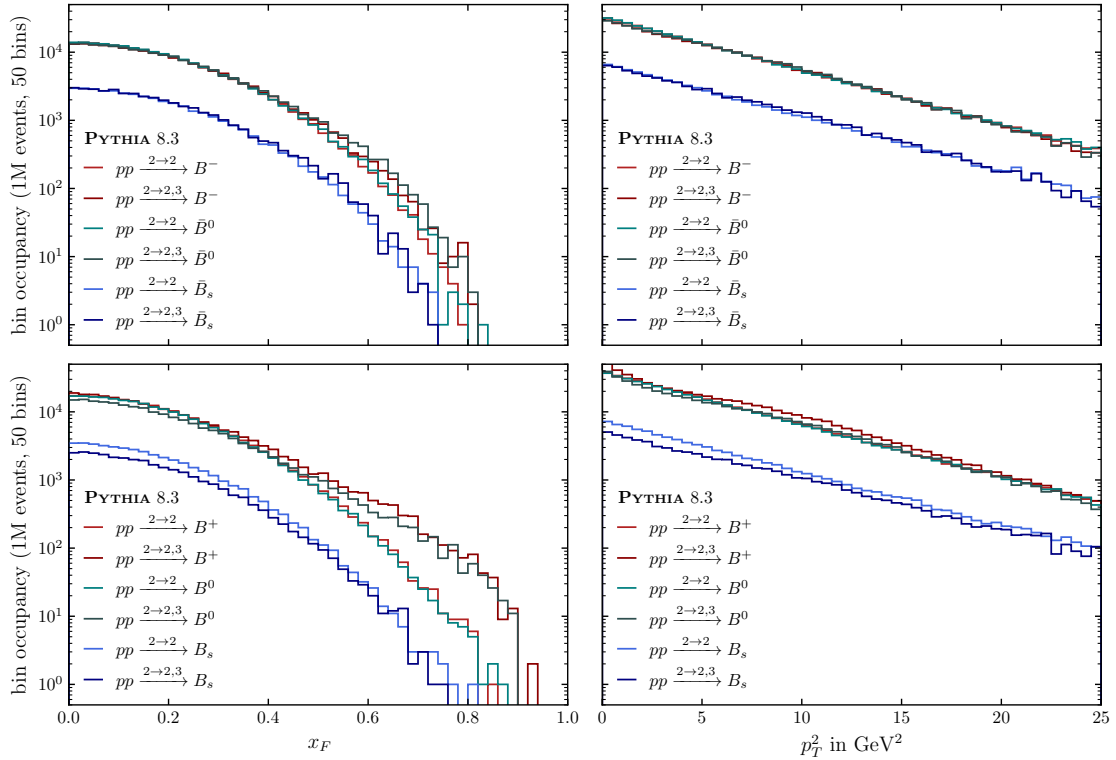


Figure 19. Comparison of x_F and p_T^2 spectra considering PYTHIA’s `HardQCD:hardbbbar` ($2 \rightarrow 2$) and a weighted combination including `HardQCD:3parton` with `HardQCD:nQuarkNew=5` ($2 \rightarrow 2, 3$) for open beauty and anti beauty mesons in the bottom and top panels respectively in $\sqrt{s} = 27.43$ GeV pp scattering.

fit	$\sigma_{c\bar{c}}$	$\sigma_{b\bar{b}}$	$n_{c\bar{c}}$	$b_{c\bar{c}}$
x scale	lin.	log.	lin.	lin.
y scale	log.	log.	lin.	lin.
σ_{amp}	0.4	5	10	10
α_{ls}	10	3	10	10
β_{ls}	1	1	1	1
$x_{\text{min}}^{\text{new}}$ in GeV	5	10	5	5
$x_{\text{max}}^{\text{new}}$ in GeV	48	20000	48	48
expected LPD	-8.9	-12.8	-15.1	-2.8

Table 6. Model details for the fits presented in section 3. For details see text.

All fits were conducted in 4 independent chains using 1000 samples each. Table 6 also gives their respective expected log pointwise predictive density (LPD) [144] as evaluated in Pareto-smoothed importance sampling leave-one-out cross-validation [145, 146], even though a reliable objective evaluation is limited due to the lack of data to compare predictions against. It also details which optimisations occurred considering the data at either a linear or logarithmic x and y ($\sigma_{q\bar{q}}$, $n_{c\bar{c}}$, and $b_{c\bar{c}}$) scales.

D Framework overview

The ALP_INIST simulation framework used to generate the FIP sensitivity estimates in this work has already been described in significant detail in previous publications [36, 37] and theses [147]. For the reader’s convenience, we summarise the basic assumptions here in appendix D.1, followed by a brief (updated) overview of the simulation chain in appendix D.2, and finally a comment on the details specific to the simulation of HNLs in appendix D.3.

D.1 Factorisation assumptions

The first underlying assumption of the ALP_INIST simulation set-up is, that the number of detected Feebly Interacting Particles as presented in eq. (2.1) can be reinterpreted as

$$N_{\text{det}}(m_X, g_X) = \int d\theta_X dE_X \frac{d^2 N^{\text{prod}}(m_X, \mathbf{g}_X)}{d\theta_X dE_X} \chi^{\text{det}}(m_X, \mathbf{g}_X, \Gamma_X, \theta_X, E_X), \quad (\text{D.1})$$

where $d^2 N^{\text{prod}}(m_X, \mathbf{g}_X)/d\theta_X dE_X$ is the spectrum of a FIP with mass m_X , SM couplings \mathbf{g}_X , and width Γ_X , with respect to the FIP energy E_X and its emission angle from the target with respect to the beam axis θ_X in the laboratory frame. The second component of this integral describes the detection probability χ^{det} of such a FIP with a given (E_X, θ_X) . In other words, we assume, that FIP production and detection factorise, which is motivated by the macroscopic on-shell propagation of the FIP from its production to the point of its decay.¹⁸

Having successfully disentangled FIP production and decay, we now observe that both production and associated decay probability can be expressed as the sum over individual channels, i.e. that the integrand of eq. (D.1) can be written as

$$\sum_i \frac{d^2 N_i^{\text{prod}}(m_X, \mathbf{g}_X)}{d\theta_X dE_X} \times \sum_f \chi_f^{\text{det}}(m_X, \mathbf{g}_X, \Gamma_X, \theta_X, E_X), \quad (\text{D.2})$$

where i denotes the i th production channel and f the f th decay channel of X . The second assumption of the simulation is now that both dN_i^{prod} and χ_f^{det} further factorise in such a way that it is possible to write

$$\frac{d^2 N_i^{\text{prod}}(m_X, \mathbf{g}_X)}{d\theta_X dE_X} = \lambda_i^{\text{prod}}(\mathbf{g}_X, \mathbf{g}_X^{\text{ref}}) \frac{d^2 N_i^{\text{prod}}(m_X, \mathbf{g}_X^{\text{ref}})}{d\theta_X dE_X} \quad (\text{D.3})$$

$$\chi_f^{\text{det}}(m_X, \mathbf{g}_X, \Gamma_X, \theta_X, E_X) = \lambda_f^{\text{dec}}(\mathbf{g}_X, \mathbf{g}_X^{\text{ref}}) \chi_f^{\text{det}}(m_X, \mathbf{g}_X^{\text{ref}}, \Gamma_X, \theta_X, E_X). \quad (\text{D.4})$$

This is to say, that the model dependence introduced by an arbitrarily chosen set of \mathbf{g}_X can be encapsulated in rescaling functions λ for a set of appropriately chosen reference

¹⁸For a nearly degenerate HNL pair this assumption does not hold, as HNL oscillations determine the breaking or conservation of Lepton number. However, in the approximation of a single HNL as presented in section 2.2, no oscillations occur, and the assumption when implemented as described in appendix D.3. We leave the implementation of oscillation phenomena to future works.

couplings $\mathbf{g}_X^{\text{ref}}$.¹⁹ Thus, we can write

$$\begin{aligned}
 N_{\text{det}} = & \sum_{i,f} \overbrace{\lambda_i^{\text{prod}}(\mathbf{g}_X, \mathbf{g}_X^{\text{ref}}) \lambda_f^{\text{dec}}(\mathbf{g}_X, \mathbf{g}_X^{\text{ref}})}^{\text{model-dependent}} \\
 & \times \underbrace{\int d\theta_X dE_X \frac{d^2 N_i^{\text{prod}}(m_X, \mathbf{g}_X^{\text{ref}})}{d\theta_X dE_X} \chi_f^{\text{det}}(m_X, \mathbf{g}_X^{\text{ref}}, \Gamma_X, \theta_X, E_X)}_{\text{kinematics and geometry}}.
 \end{aligned}
 \tag{D.5}$$

In this way, if the mass m_X and the total width Γ_X are treated as free parameters, N_{det} can be factorised into a model-dependent part, and a second part determined only by the kinematics of X and the experimental geometry.

D.2 Structural layout

The ALPiNIST framework is built around the idea that the number of detectable events of Beyond Standard Model decays at a beam-dump experiments factorises into a kinematic and a model-dependent part as presented in section D.1. It can be summarised as presented in figure 20, with boxes representing code elements and triangles the tables for intermediate data storage with the orientation indicating the direction of data flow.²⁰ The three major modular simulation components are related to the components of eq. (D.5) as given in table 7. The individual parts and their function will be described in more detail below.

<code>EXO_production</code>	calculates the spectrum $\frac{d^2 N_i}{d\theta_X dE_X}$ for a given production channel i ;
<code>EXO_decay</code>	calculates yields for decay channels f for each production spectrum $d^2 N_i$;
<code>EXO_rescale</code>	performs the appropriate rescaling $\lambda_i^{\text{prod}}(\mathbf{g}_X, \mathbf{g}_X^{\text{ref}}) \lambda_f^{\text{dec}}(\mathbf{g}_X, \mathbf{g}_X^{\text{ref}})$ for the relevant channels and consequently sums over the individual yields.

Table 7. Summary of the main ALPiNIST module functionalities.

The `EXO_production` module is written in PYTHON 3 and uses functionalities of the ROOT framework [148]. It emulates the beam particle’s interaction with the target material leading to the production of a feebly interacting particle. As FIP production can occur in primary or secondary interactions, for some production channels intermediate Standard Model states are required. These are typically light or heavy mesons which mix with or decay into the FIP. Their momentum distributions can be calculated using either the directly interfaced PYTHIA 8 [149], from implemented empirical distributions relying on experimental data, or any other an external generator when provided as a data table. For several

¹⁹Note that λ generally relates the relevant branching fraction to the reference coupling. This also ensures that the rescaled χ^{det} can never exceed 1.

²⁰Given the appropriate inputs, FIPs of alternative origins can also be studied skipping the production module in the simulation chain presented in figure 20.

tables of expected yield in terms of mass and coupling strength, sensitivity plots in various FIP parameter representations, and the respective tabulated contours.

D.3 Simulating Heavy Neutral Leptons

The ALP_INIST simulation method relies on the underlying assumption that the production and decay of the Feebly Interacting Particle can be treated independent of one another (c.f. appendix D.1). For a degenerate pair of HNLs undergoing oscillations, this is not necessarily the case. But even for a single HNL described by the phenomenological seesaw interactions (see section 2.2), this is not always the case. In ALP_INIST, at the kinematic level, we treat electronphilic, muonphilic and tauphilic mixing as separate production channels. This allows us to simulate decay channels of the HNL based on the three production spectra. The overall yields for this channel is then the incoherent sum of the three yields based on the HNL’s coupling ratios. For two-body decays this approach is fully justified, as the coupling factorises from the kinematic description of the decays. However, for three-body decays of the type $N \rightarrow \nu \ell \ell^{(\prime)}$, the exact kinematic distribution of the decay products depends on the coupling structure (i.e. the Dalitz plot of the tauphilic decay into $\nu_e e \bar{e}$ differs from that of the electronphilic decay into the related channel $\nu_\tau e \bar{e}$). This is due to the HNL being able to couple both via neutral or charged current as shown in figure 15 and the contributions possibly adding coherently. Consequently, one would have to simulate not only $\nu e e$ for the three different production spectra, but $\nu_e e \bar{e}$ and $\nu_{\mu/\tau} e \bar{e}$, increasing the total number of combinations to three-body leptonic decays with only e and μ in the final state from 9 to 18.

In practise, however, we find that the exact kinematic distribution of the three-body HNL decays has little influence on the final sensitivities. In order to reduce the amount of necessary simulations, we therefore limit ourselves to simulating the decays using the Dalitz distributions according to the active coupling production spectrum.²² This ensures, that the trivial benchmark cases are simulated with the exact kinematics, while the error resulting for admixtures of HNLs is comparable to the difference presented in previous works [147] (often below statistical fluctuations).

E Further sensitivity comparisons

E.1 NA62 experiment in beam-dump mode

A commonly cited reference for the prospect sensitivity of the NA62 sensitivity in beam-dump mode is the study by Drewes et al. [151]. This study employed a toy MC with decay products required to be within acceptance of the charged hodoscope. Moreover, the study of [151] states that the composition of the shower and the kinematics of the produced c- and b-hadrons were obtained by simulating the 400 GeV proton beam on a thick (~ 11 interaction lengths) high-Z target with Pythia 6.4. Our results of figure 11 suggest weaker sensitivity for the NA62 experiment in beam-dump mode than estimated in [151]. We

²²In ALP_INIST, the simulations can alternatively be performed using flat Dalitz distributions instead by invoking the `--flat-dalitz` flag.

would like to note however, that using the differential cross sections of charmed mesons measured by the LEBC-EHS collaboration [80], we reproduce results similar to those by Drewes et al. [151]. Similarly to the analyses of di-lepton searches [103, 104], the NA62-BD data can also be analysed for the possibility of HNL decays. This would make both projections obsolete in the future.

E.2 SHiP experiment

Since its first inception, the concept design of the SHiP experiment has undergone major changes. In this section we present the ALPiNIST sensitivity estimates for the latest implementation, following the latest proposal by the BDF/SHiP collaboration [8], the key parameters of which are summarised in table 4. We include in our comparisons estimates of the semi-analytic light-weight-MC SENSALC [39] which has been widely employed in phenomenological studies of SHiP sensitivities.²³

Important components of the SHiP experiment are a $4 \times 6 \text{ m}^2$ spectrometer system just behind the decay volume (DV), featuring a $162.5 \text{ mT} \times 4 \text{ m}$ magnet. Further downstream, the $5.3 \times 6.7 \text{ m}^2$ electromagnetic calorimeter, and a subsequent $5.2 \times 6.6 \text{ m}^2$ muon/hadronic calorimeter are foreseen. Beyond the resulting geometrical cuts, we use the signal cuts as prescribed by BDF/SHiP [8] on final state kinematics

1. $1 \text{ GeV c}^{-1} < p_{\text{track}},$
2. $\min |\vec{r}_{\text{vtx2}} - \vec{r}_{\text{DVwall}}| > 5 \text{ cm},$

which demands that all observable final state particles have a momentum greater than 1 GeV c^{-1} and the reconstructed decay vertex be 5 cm away from the inner wall of the decay volume. These are complemented for decay channels including a neutrino by the additional requirements

3. $z_{\text{vtx2}} - z_{\text{DV}} > 1 \text{ m},$
4. $b_{\text{target}} < 2.5 \text{ m}.$

Here, b_{target} is the impact parameter of the reconstructed FIP track with respect to the beam axis at the interaction point.

The resulting parameter sensitivities for electronphilic, muonphilic, and tauphilic HNLs are presented in figure 21. In all three scenarios, the estimates are in reasonable agreement with the literature values [8]. Just above the 1 GeV threshold the predictions including all possible final states of SENSALC and ALPiNIST diverge in all Benchmark Cases. This is due to the fact, that in this regime semileptonic decays including multiple hadrons begin to dominate the total width. SENSALC models these as decays into quarks with subsequent hadronisation, while ALPiNIST considers only the final states with a single meson as

²³We used v1.0.6.1 to reproduce the BDF/SHiP results [8]. We adjusted the mass step sizes with respect to the standard settings of this version resulting in slight differences between contours. This, as well as improved calculation of the decay products acceptance are implemented in versions after v1.1.2.1, leading to the dashed teal sensitivity curves presented in figure 21.

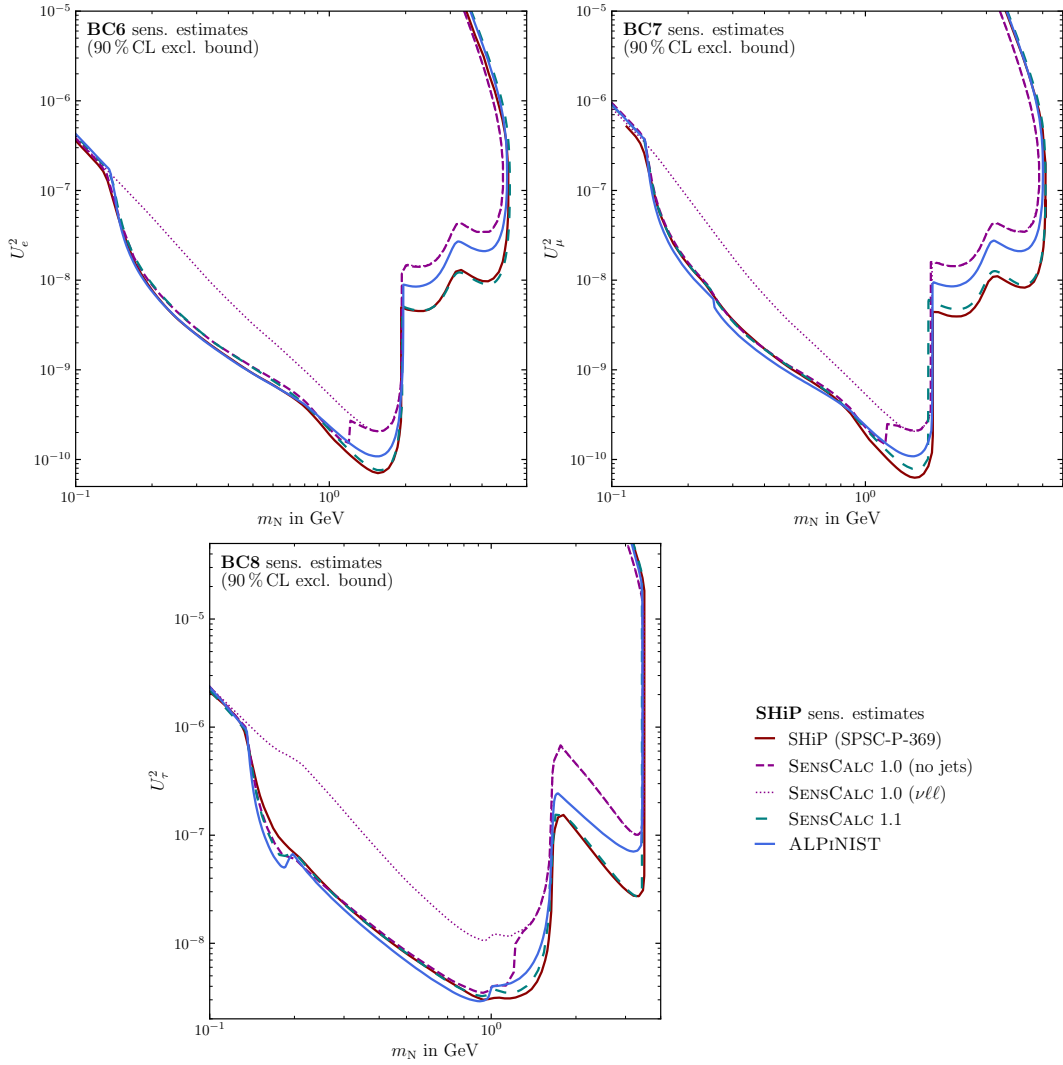


Figure 21. Predicted sensitivity (90% CL excl. bound) for a electronphilic (top left), muonphilic (top right) and tauphilic (bottom) HNLs of the SHiP experiment at ECN3. The red lines show the published prediction by the BDF/SHiP collaboration [8], relying on the semi-analytic light-weight-MC SENSICALC [39]. Using the same tool, but not including hadronising open-quark-final-states (hadronic final states) as signal results in the purple dashed (dotted) line. The dashed teal curves show the expectation using the latest version of SENSICALC available as of the writing of this paper, considering all available final states as signal. The blue solid lines show the ALPiNIST prediction using the same meson inputs as SENSICALC [51].

signal, taking multi-hadron final states into account only as a contribution to the total HNL decay width as presented in section A.2. Above this threshold, the purple dashed lines showcase the sensitivity to only fully leptonic decays and are in reasonable agreement with the ALPiNIST generated curves. Another point of disagreement is the sensitivity just below $m_N = 200$ MeV in the tauphilic case, where the decay chain $D_s \rightarrow \tau(N \rightarrow \pi\nu)$ gives the dominant contribution to the sensitivity. This disagreement is less significant

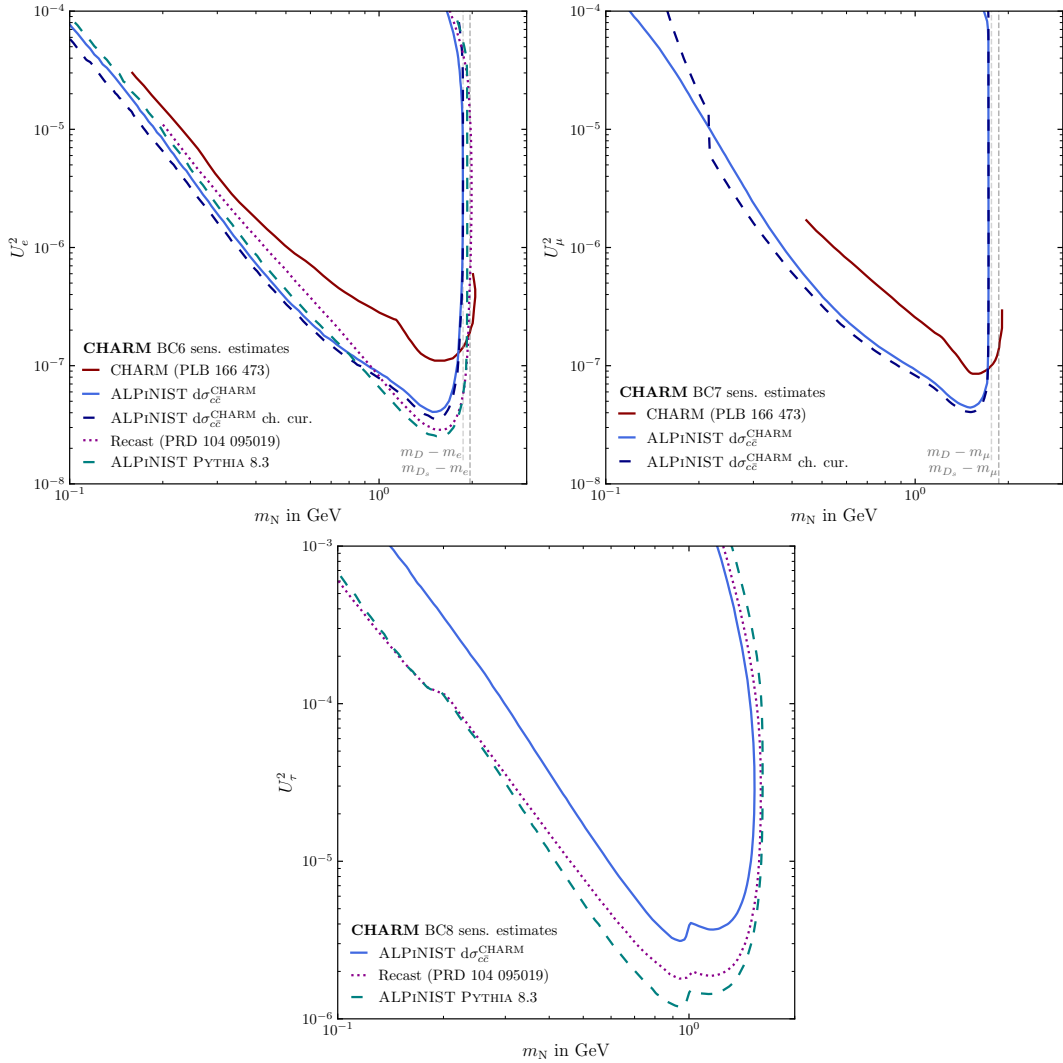


Figure 22. Comparison of the CHARM experiments HNL sensitivity estimates (90% CL excl. bound) using ALPiNIST to those by the CHARM collaboration [97] and a more recent recast of the search [50]. Note that the ALPiNIST curves using the $d\sigma_{cc}^{\text{CHARM}}$ differential production cross sections do not contain contributions from D_s mesons [97] relevant above $m_N \simeq 600$ MeV for BC6 and BC7, and at all masses for BC8.

with our evaluation using SENSALC.²³

E.3 CHARM experiment

In the scenario of electron and muon-coupling dominance, one of the strongest HNL exclusions is set by a search performed by the CHARM experiment.²⁴ Around 2×10^{18} protons of 400 GeV were dumped onto a thick copper beam-dump. A search was performed looking for visible decays with electrons/muons in the final state in the 35 m long decay volume [97].

²⁴These results are complemented by a re-interpretation of the CHARM limits in terms of τ couplings through a recast [50].

In order to validate ALP_INIST against this limit, some understanding of the shape and overall numbers of D-mesons assumed in the analysis is needed. In the final version of the search [97], the input assumption for N_D (the number of D mesons produced in the dump) is mentioned only as scaling with another measured quantity, not as an absolute number. The scaling procedure is explained in an earlier publication by CHARM from 1983 [98]. It takes as a reference the number of prompt single-muon events observed in the CHARM calorimeter in order to infer N_D . In terms of differential D meson distribution, CHARM quote eq. (3.1) with $a = 2$, $b = 0$, and where in the earlier paper [98], the x_F exponent is taken to be 4, while in ref. [97], 5 is assumed.

While we are able to re-reproduce the overall shape of the CHARM exclusion²⁵, the absolute value of the contour is not reproducible with our understanding of the $d\sigma_{cc}$ assumed. We attribute this to the fact that we are unable to fully follow the scaling procedure proposed in ref. [98], given the very satisfactory reproduction of the BEBC limit with ALP_INIST.

Figure 22 shows a comparison between the sensitivity estimate for the CHARM experiment to HNLs using ALP_INIST and literature. The differential production cross section used in an attempt to replicate the data published by the CHARM collaboration match those presented in said publication [97]. The blue ALP_INIST curves are presented using production exclusively from D^\pm and D^0 mesons with only charged current (ch. cur.), as well as also including neutral current mediated decays of the HNL. To compare to a more modern recast of the experiment’s results [50], we also present the ALP_INIST curves as given by PYTHIA 8.3 including production from D_s mesons.

References

- [1] J. Beacham et al., *Physics Beyond Colliders at CERN: Beyond the Standard Model Working Group Report*, *J. Phys. G* **47** (2020), no. 1 010501, [[1901.09966](#)].
- [2] C. Antel et al., *Feebly Interacting Particles: FIPs 2022 workshop report*, *Eur. Phys. J. C* **83** (2023) 1122, [[2305.01715](#)].
- [3] **IAXO Collaboration**, A. Abeln et al., *Conceptual design of BabyIAXO, the intermediate stage towards the International Axion Observatory*, *JHEP* **05** (2021) 137, [[2010.12076](#)].
- [4] B. Dutta, W.-C. Huang, D. Kim, J. L. Newstead, J.-C. Park, et al., *Exciting Prospects for Dark Matter at Large-Volume Neutrino Detectors*, [2402.04184](#).
- [5] **FASER Collaboration**, A. Ariga et al., *FASER’s physics reach for long-lived particles*, *Phys. Rev. D* **99** (2019), no. 9 095011, [[1811.12522](#)].
- [6] V. Gorkavenko, B. Jashal, V. Kholoimov, Y. Kyselov, D. Mendoza, et al., *LHCb potential to discover long-lived new physics particles with lifetimes above 100 ps*, [2312.14016](#).
- [7] **MATHUSLA Collaboration**, C. Alpigiani et al., *A Letter of Intent for MATHUSLA: A Dedicated Displaced Vertex Detector above ATLAS or CMS*, [1811.00927](#).

²⁵We would like to observe that the quality of the printed contour limit at large masses (~ 2 GeV) in figures 2,3 of [97], including the BEBC contour, do not exactly facilitate the contour validation. Partially, limits seem to have been drawn beyond ~ 2 GeV, in contrast to the performed measurements and what is kinematically possible.

- [8] **SHiP Collaboration**, R. Albanese, J. Alt, A. Alexandrov, S. Aoki, D. Arutinov, et al., *BDF/SHiP at the ECN3 high-intensity beam facility*, tech. rep., CERN, Geneva, 2023.
- [9] **SHADOWS Collaboration**, M. Alviggi, S. Bachmann, W. Baldini, A. Balla, M. Barth, et al., *SHADOWS Technical Proposal*, tech. rep., CERN, Geneva, 2023.
- [10] **HIKE Collaboration**, M. U. Ashraf et al., *High Intensity Kaon Experiments (HIKE) at the CERN SPS Proposal for Phases 1 and 2*, [2311.08231](#).
- [11] P. Giffin, S. Gori, Y.-D. Tsai, and D. Tuckler, *Heavy neutral leptons at beam dump experiments of future lepton colliders*, *JHEP* **04** (2023) 046, [[2206.13745](#)].
- [12] **CHARM Collaboration**, M. Jonker et al., *Experimental Study of Neutral Current and Charged Current Neutrino Cross-Sections*, *Phys. Lett. B* **99** (1981) 265. [Erratum: *Phys.Lett.B* 100, 520 (1981), Erratum: *Phys.Lett.B* 103, 469 (1981)].
- [13] **CCFR/NuTeV Collaboration**, A. Romosan et al., *A High statistics search for muon-neutrino (anti-muon-neutrino) \rightarrow electron-neutrino (anti-electron-neutrino) oscillations in the small mixing angle regime*, *Phys. Rev. Lett.* **78** (1997) 2912–2915, [[hep-ex/9611013](#)].
- [14] **DUNE Collaboration**, B. Abi et al., *Prospects for beyond the Standard Model physics searches at the Deep Underground Neutrino Experiment*, *Eur. Phys. J. C* **81** (2021), no. 4 322, [[2008.12769](#)].
- [15] **NA62 Collaboration**, E. Cortina Gil et al., *The Beam and detector of the NA62 experiment at CERN*, *JINST* **12** (2017), no. 05 P05025, [[1703.08501](#)].
- [16] **PIONEER Collaboration**, W. Altmannshofer et al., *PIONEER: Studies of Rare Pion Decays*, [2203.01981](#).
- [17] P. Minkowski, *$\mu \rightarrow e\gamma$ at a Rate of One Out of 10^9 Muon Decays?*, *Phys. Lett. B* **67** (1977) 421–428.
- [18] M. Gell-Mann, P. Ramond, and R. Slansky, *Complex Spinors and Unified Theories*, *Conf. Proc. C* **790927** (1979) 315–321, [[1306.4669](#)].
- [19] M. Shaposhnikov, *A Possible symmetry of the nuMSM*, *Nucl. Phys. B* **763** (2007) 49–59, [[hep-ph/0605047](#)].
- [20] S. Dodelson and L. M. Widrow, *Sterile-neutrinos as dark matter*, *Phys. Rev. Lett.* **72** (1994) 17–20, [[hep-ph/9303287](#)].
- [21] X.-D. Shi and G. M. Fuller, *A New dark matter candidate: Nonthermal sterile neutrinos*, *Phys. Rev. Lett.* **82** (1999) 2832–2835, [[astro-ph/9810076](#)].
- [22] K. Abazajian, G. M. Fuller, and M. Patel, *Sterile neutrino hot, warm, and cold dark matter*, *Phys. Rev. D* **64** (2001) 023501, [[astro-ph/0101524](#)].
- [23] T. Asaka, M. Laine, and M. Shaposhnikov, *Lightest sterile neutrino abundance within the nuMSM*, *JHEP* **01** (2007) 091, [[hep-ph/0612182](#)]. [Erratum: *JHEP* 02, 028 (2015)].
- [24] A. Boyarsky, O. Ruchayskiy, and M. Shaposhnikov, *The Role of sterile neutrinos in cosmology and astrophysics*, *Ann. Rev. Nucl. Part. Sci.* **59** (2009) 191–214, [[0901.0011](#)].
- [25] M. Fukugita and T. Yanagida, *Baryogenesis Without Grand Unification*, *Phys. Lett. B* **174** (1986) 45–47.
- [26] E. K. Akhmedov, V. A. Rubakov, and A. Y. Smirnov, *Baryogenesis via neutrino oscillations*, *Phys. Rev. Lett.* **81** (1998) 1359–1362, [[hep-ph/9803255](#)].

- [27] T. Asaka and M. Shaposhnikov, *The ν MSM, dark matter and baryon asymmetry of the universe*, *Phys. Lett. B* **620** (2005) 17–26, [[hep-ph/0505013](#)].
- [28] J. Klarić, M. Shaposhnikov, and I. Timiryasov, *Reconciling resonant leptogenesis and baryogenesis via neutrino oscillations*, *Phys. Rev. D* **104** (2021), no. 5 055010, [[2103.16545](#)].
- [29] M. Drewes, Y. Georis, and J. Klarić, *Mapping the Viable Parameter Space for Testable Leptogenesis*, *Phys. Rev. Lett.* **128** (2022), no. 5 051801, [[2106.16226](#)].
- [30] S. N. N. L. Constraints. www.sterile-neutrino.org.
- [31] **SHiPcollaboration Collaboration**, T. Ruf and H. Dijkstra, *Heavy Flavour Cascade Production in a Beam Dump*, .
- [32] V. M. Gorkavenko, Y. R. Borysenkova, and M. S. Tsarenkova, *Production of GeV-scale heavy neutral leptons in three-body decays. Comparison with the PYTHIA approach*, *J. Phys. G* **48** (2021), no. 10 105001, [[2103.11494](#)].
- [33] B. Döbrich, J. Jaeckel, and T. Spadaro, *Light in the beam dump - ALP production from decay photons in proton beam-dumps*, *JHEP* **05** (2019) 213, [[1904.02091](#)]. [Erratum: *JHEP* 10, 046 (2020)].
- [34] C. Lourenco and H. K. Wohri, *Heavy flavour hadro-production from fixed-target to collider energies*, *Phys. Rept.* **433** (2006) 127–180, [[hep-ph/0609101](#)].
- [35] **SHiP Collaboration**, C. Ahdida et al., *Reconstruction of 400 GeV/c proton interactions with the SHiP-charm project*, *Eur. Phys. J. C* **84** (2024), no. 6 562, [[2406.04730](#)].
- [36] J. Jerhot, B. Döbrich, F. Ertas, F. Kahlhoefer, and T. Spadaro, *ALPINIST: Axion-Like Particles In Numerous Interactions Simulated and Tabulated*, *JHEP* **07** (2022) 094, [[2201.05170](#)].
- [37] Y. Afik, B. Döbrich, J. Jerhot, Y. Soreq, and K. Tobioka, *Probing long-lived axions at the KOTO experiment*, *Phys. Rev. D* **108** (2023), no. 5 055007, [[2303.01521](#)].
- [38] L. Buonocore, C. Frugiuele, F. Maltoni, O. Mattelaer, and F. Tramontano, *Event generation for beam dump experiments*, *JHEP* **05** (2019) 028, [[1812.06771](#)].
- [39] M. Ovchinnikov, J.-L. Tastet, O. Mikulenko, and K. Bondarenko, *Sensitivities to feebly interacting particles: Public and unified calculations*, *Phys. Rev. D* **108** (2023), no. 7 075028, [[2305.13383](#)].
- [40] F. Domingo, J. Günther, J. S. Kim, and Z. S. Wang, *A C++ program for estimating detector sensitivities to long-lived particles: Displaced Decay Counter*, [2308.07371](#).
- [41] B. Dobrich, *Exotic particle searches at beam-dumps – dos and don’ts*, *PoS WIFAI2023* (2024) 012.
- [42] A. M. Abdullahi et al., *The present and future status of heavy neutral leptons*, *J. Phys. G* **50** (2023), no. 2 020501, [[2203.08039](#)].
- [43] K. Bondarenko, A. Boyarsky, D. Gorbunov, and O. Ruchayskiy, *Phenomenology of GeV-scale Heavy Neutral Leptons*, *JHEP* **11** (2018) 032, [[1805.08567](#)].
- [44] R. E. Shrock, *General Theory of Weak Leptonic and Semileptonic Decays. 1. Leptonic Pseudoscalar Meson Decays, with Associated Tests For, and Bounds on, Neutrino Masses and Lepton Mixing*, *Phys. Rev. D* **24** (1981) 1232.

- [45] R. E. Shrock, *General Theory of Weak Processes Involving Neutrinos. 2. Pure Leptonic Decays*, *Phys. Rev. D* **24** (1981) 1275.
- [46] L. M. Johnson, D. W. McKay, and T. Bolton, *Extending sensitivity for low mass neutral heavy lepton searches*, *Phys. Rev. D* **56** (1997) 2970–2981, [[hep-ph/9703333](#)].
- [47] D. Gorbunov and M. Shaposhnikov, *How to find neutral leptons of the ν MSM?*, *JHEP* **10** (2007) 015, [[0705.1729](#)]. [Erratum: *JHEP* 11, 101 (2013)].
- [48] A. Atre, T. Han, S. Pascoli, and B. Zhang, *The Search for Heavy Majorana Neutrinos*, *JHEP* **05** (2009) 030, [[0901.3589](#)].
- [49] O. Ruchayskiy and A. Ivashko, *Experimental bounds on sterile neutrino mixing angles*, *JHEP* **06** (2012) 100, [[1112.3319](#)].
- [50] I. Boiarska, A. Boyarsky, O. Mikulenko, and M. Ovchinnikov, *Constraints from the charm experiment on heavy neutral leptons with tau mixing*, *Phys. Rev. D* **104** (Nov, 2021) 095019.
- [51] **SHiP Collaboration**, T. Ruf and H. Dijkstra, *Heavy Flavour Cascade Production in a Beam Dump*, .
- [52] **DUNE Collaboration**, Z. G. Moghaddam, *Sensitivity to Heavy Neutral Leptons with the SAND detector at the DUNE ND complex*, [2209.01899](#).
- [53] M. Fieg, F. Kling, H. Schulz, and T. Sjöstrand, *Tuning pythia for forward physics experiments*, *Phys. Rev. D* **109** (2024), no. 1 016010, [[2309.08604](#)].
- [54] R. Vogt, *The Total charm cross-section*, *Eur. Phys. J. ST* **155** (2008) 213–222, [[0709.2531](#)].
- [55] M. Cacciari, M. Greco, and P. Nason, *The p_T spectrum in heavy-flavour hadroproduction.*, *JHEP* **05** (1998) 007, [[hep-ph/9803400](#)].
- [56] M. Cacciari, S. Frixione, and P. Nason, *The $p(T)$ spectrum in heavy flavor photoproduction*, *JHEP* **03** (2001) 006, [[hep-ph/0102134](#)].
- [57] A. Buckley, J. Ferrando, S. Lloyd, K. Nordström, B. Page, et al., *LHAPDF6: parton density access in the LHC precision era*, *Eur. Phys. J. C* **75** (2015) 132, [[1412.7420](#)].
- [58] **NNPDF Collaboration**, R. D. Ball et al., *The path to proton structure at 1% accuracy*, *Eur. Phys. J. C* **82** (2022), no. 5 428, [[2109.02653](#)].
- [59] S. Frixione, M. L. Mangano, P. Nason, and G. Ridolfi, *Charm and bottom production: Theoretical results versus experimental data*, *Nucl. Phys. B* **431** (1994) 453–483.
- [60] O. Abril-Pla, V. Andreani, C. Carroll, L. Dong, C. J. Fonnesebeck, et al., *Pymc: a modern, and comprehensive probabilistic programming framework in python*, *PeerJ Computer Science* **9** (Sept., 2023) e1516.
- [61] **SVD-2 Collaboration**, A. Aleev et al., *Charmed particles production in pA -interactions at $\sqrt{s} = 11.8$ GeV*, *Eur. Phys. J. A* **53** (2017), no. 3 45.
- [62] **ACCMOR Collaboration**, S. Barlag et al., *Production of D , D^* and $D(s)$ Mesons in 200-GeV/c π^- , K^- and p Si Interactions*, *Z. Phys. C* **39** (1988) 451.
- [63] **E769 Collaboration**, G. A. Alves et al., *Forward cross-sections for production of D^+ , D^0 , $D(s)$, D^{*+} and $\Lambda(c)$ in 250-GeV π^{+-} , K^{+-} , and p - nucleon interactions*, *Phys. Rev. Lett.* **77** (1996) 2388–2391. [Erratum: *Phys.Rev.Lett.* 81, 1537 (1998)].

- [64] M. Adamovich et al., *Results on charm physics from WA82*, *Nucl. Phys. B Proc. Suppl.* **27** (1992) 212–218.
- [65] **LEBC-EHS Collaboration**, M. Aguilar-Benitez et al., *D Meson Branching Ratios and Hadronic Charm Production Cross-sections*, *Phys. Lett. B* **135** (1984) 237–242.
- [66] **LEBC-EHS Collaboration**, M. Aguilar-Benitez et al., *Charm Hadron Properties in 400-GeV/c p p Interactions*, *Z. Phys. C* **40** (1988) 321.
- [67] R. Ammar et al., *D-Meson Production in 800-GeV/c p Pinteractions*, *Phys. Rev. Lett.* **61** (1988) 2185–2188.
- [68] **Fermilab E653 Collaboration**, K. Kodama et al., *Charm Meson Production in 800-GeV/c Proton - Emulsion Interactions*, *Phys. Lett. B* **263** (1991) 573–578.
- [69] **HERA-B Collaboration**, I. Abt et al., *Measurement of D0, D+, D+(s) and D*+ Production in Fixed Target 920-GeV Proton-Nucleus Collisions*, *Eur. Phys. J. C* **52** (2007) 531–542, [[0708.1443](#)].
- [70] **E789 Collaboration**, M. J. Leitch et al., *Nuclear dependence of neutral D meson production by 800-GeV/c protons*, *Phys. Rev. Lett.* **72** (1994) 2542–2545.
- [71] D. M. Jansen et al., *Measurement of the bottom quark production cross-section in 800-GeV/c proton - gold collisions*, *Phys. Rev. Lett.* **74** (1995) 3118–3121.
- [72] **HERA-B Collaboration**, I. Abt et al., *Improved measurement of the b-anti-b production cross section in 920-GeV fixed-target proton-nucleus collisions*, *Phys. Rev. D* **73** (2006) 052005, [[hep-ex/0512030](#)].
- [73] **PHENIX Collaboration**, C. Aidala et al., *Measurements of $\mu\mu$ pairs from open heavy flavor and Drell-Yan in p + p collisions at $\sqrt{s} = 200$ GeV*, *Phys. Rev. D* **99** (2019), no. 7 072003, [[1805.02448](#)].
- [74] **PHENIX Collaboration**, U. Acharya et al., *Production of $b\bar{b}$ at forward rapidity in p+p collisions at $\sqrt{s} = 510$ GeV*, *Phys. Rev. D* **102** (2020), no. 9 092002, [[2005.14276](#)].
- [75] **UA1 Collaboration**, C. Albajar et al., *Beauty production at the CERN p anti-p collider*, *Phys. Lett. B* **256** (1991) 121–128. [Erratum: *Phys.Lett.B* 262, 497 (1991)].
- [76] **ALICE Collaboration**, B. Abelev et al., *Measurement of electrons from beauty hadron decays in pp collisions at $\sqrt{s} = 7$ TeV*, *Phys. Lett. B* **721** (2013) 13–23, [[1208.1902](#)]. [Erratum: *Phys.Lett.B* 763, 507–509 (2016)].
- [77] **LHCb Collaboration**, R. Aaij et al., *Measurement of $\sigma(pp \rightarrow b\bar{b}X)$ at $\sqrt{s} = 7$ TeV in the forward region*, *Phys. Lett. B* **694** (2010) 209–216, [[1009.2731](#)].
- [78] **LHCb Collaboration**, R. Aaij et al., *Measurement of the b-quark production cross-section in 7 and 13 TeV pp collisions*, *Phys. Rev. Lett.* **118** (2017), no. 5 052002, [[1612.05140](#)]. [Erratum: *Phys.Rev.Lett.* 119, 169901 (2017)].
- [79] **Particle Data Group Collaboration**, R. L. Workman et al., *Review of Particle Physics*, *PTEP* **2022** (2022) 083C01.
- [80] **LEBC-EHS Collaboration**, M. Aguilar-Benitez et al., *D Meson Production From 400 GeV/cpp Interactions*, *Phys. Lett. B* **189** (1987) 476. [Erratum: *Phys.Lett.B* 208, 530 (1988)].
- [81] **CHARM Collaboration**, F. Bergsma, *Charm production measured in a 400-GeV proton copper beam dump experiment*, *Annals N. Y. Acad. Sci.* **535** (1988) 506–515.

- [82] D. Boyanovsky, *Nearly degenerate heavy sterile neutrinos in cascade decay: mixing and oscillations*, *Phys. Rev. D* **90** (2014), no. 10 105024, [[1409.4265](#)].
- [83] J.-L. Tastet and I. Timiryasov, *Dirac vs. Majorana HNLs (and their oscillations) at SHiP*, *JHEP* **04** (2020) 005, [[1912.05520](#)].
- [84] O. Mikulenko, K. Bondarenko, A. Boyarsky, and O. Ruchayskiy, *Unveiling new physics with discoveries at Intensity Frontier*, [2312.05163](#).
- [85] J. Jerhot, B. Döbrich, E. Ertas, F. Kahlhoefer, and T. Spadaro, *ALPINIST: v1.0.0*, .
- [86] G. G. Harigel, *List of publications covering BEBC experiments*. CERN Yellow Reports: Monographs. CERN, Geneva, 1985.
- [87] **BEBC WA66 Collaboration**, H. Grassler et al., *Prompt Neutrino Production in 400-GeV Proton Copper Interactions*, *Nucl. Phys. B* **273** (1986) 253–274.
- [88] H. Foeth, *The internal picket fence for bebc*, *Nuclear Instruments and Methods* **176** (1980), no. 1 203–206.
- [89] F. Wittgenstein, *Preliminary Test Results of BEBC Superconducting Magnet*, *eConf C720919* (1972) 295.
- [90] W. K. Sakumoto et al., *Calibration of the CCFR Target Calorimeter*, *Nucl. Instrum. Meth. A* **294** (1990) 179–192.
- [91] B. J. King et al., *Measuring Muon Momenta with the CCFR Neutrino Detector*, *Nucl. Instrum. Meth. A* **302** (1991) 254–260.
- [92] **NuTeV, E815 Collaboration**, A. Vaitaitis et al., *Search for neutral heavy leptons in a high-energy neutrino beam*, *Phys. Rev. Lett.* **83** (1999) 4943–4946, [[hep-ex/9908011](#)].
- [93] W. would like to thank S. Gori for providing us with the PDF of this APS contribution. <https://meetings.aps.org/Meeting/APR24/Session/D14.5>.
- [94] C. P. study group presentation. https://indico.cern.ch/event/1369776/contributions/5760315/attachments/2825823/4936322/PBC_introduction.pdf.
- [95] **WA66 Collaboration**, A. M. Cooper-Sarkar et al., *Search for Heavy Neutrino Decays in the BEBC Beam Dump Experiment*, *Phys. Lett. B* **160** (1985) 207–211.
- [96] R. Barouki, G. Marocco, and S. Sarkar, *Blast from the past II: Constraints on heavy neutral leptons from the BEBC WA66 beam dump experiment*, *SciPost Phys.* **13** (2022) 118, [[2208.00416](#)].
- [97] **CHARM Collaboration**, F. Bergsma et al., *A Search for Decays of Heavy Neutrinos in the Mass Range 0.5-GeV to 2.8-GeV*, *Phys. Lett. B* **166** (1986) 473–478.
- [98] F. Bergsma, J. Dorenbosch, M. Jonker, C. Nieuwenhuis, J. Allaby, et al., *A search for decays of heavy neutrinos*, *Physics Letters B* **128** (1983), no. 5 361–366.
- [99] J. Carvalho, *Compilation of cross sections for proton nucleus interactions at the HERA energy*, *Nucl. Phys. A* **725** (2003) 269–275.
- [100] P. D. Group, R. L. Workman, V. D. Burkert, V. Crede, E. Klempt, et al., *Review of Particle Physics*, *Progress of Theoretical and Experimental Physics* **2022** (08, 2022) 083C01, [<https://academic.oup.com/ptep/article-pdf/2022/8/083C01/49175539/ptac097.pdf>].
- [101] J. M. Berryman, A. de Gouvea, P. J. Fox, B. J. Kayser, K. J. Kelly, et al., *Searches for*

- Decays of New Particles in the DUNE Multi-Purpose Near Detector*, *JHEP* **02** (2020) 174, [[1912.07622](#)].
- [102] **DUNE Collaboration**, V. Hewes et al., *Deep Underground Neutrino Experiment (DUNE) Near Detector Conceptual Design Report*, *Instruments* **5** (2021), no. 4 31, [[2103.13910](#)].
- [103] **NA62 Collaboration**, E. Cortina Gil et al., *Search for dark photon decays to $\mu^+\mu^-$ at NA62*, *JHEP* **09** (2023) 035, [[2303.08666](#)].
- [104] **NA62 Collaboration**, E. Cortina Gil et al., *Search for leptonic decays of the dark photon at NA62*, [2312.12055](#).
- [105] B. Batell, J. A. Evans, S. Gori, and M. Rai, *Dark Scalars and Heavy Neutral Leptons at DarkQuest*, *JHEP* **05** (2021) 049, [[2008.08108](#)].
- [106] G. Bernardi et al., *FURTHER LIMITS ON HEAVY NEUTRINO COUPLINGS*, *Phys. Lett. B* **203** (1988) 332–334.
- [107] **E949 Collaboration**, A. V. Artamonov et al., *Search for heavy neutrinos in $K^+ \rightarrow \mu^+\nu_H$ decays*, *Phys. Rev. D* **91** (2015), no. 5 052001, [[1411.3963](#)]. [Erratum: *Phys.Rev.D* 91, 059903 (2015)].
- [108] R. S. Hayano et al., *HEAVY NEUTRINO SEARCH USING $K(\mu 2)$ DECAY*, *Phys. Rev. Lett.* **49** (1982) 1305.
- [109] T. Yamazaki et al., *Search for Heavy Neutrinos in Kaon Decay*, *Conf. Proc. C* **840719** (1984) 262.
- [110] **PIENU Collaboration**, A. Aguilar-Arevalo et al., *Search for heavy neutrinos in $\pi \rightarrow \mu\nu$ decay*, *Phys. Lett. B* **798** (2019) 134980, [[1904.03269](#)].
- [111] **T2K Collaboration**, K. Abe et al., *Search for heavy neutrinos with the T2K near detector ND280*, *Phys. Rev. D* **100** (2019), no. 5 052006, [[1902.07598](#)].
- [112] **NA62 Collaboration**, E. Cortina Gil et al., *Search for heavy neutral lepton production in K^+ decays to positrons*, *Phys. Lett. B* **807** (2020) 135599, [[2005.09575](#)].
- [113] **NA62 Collaboration**, E. Cortina Gil et al., *Search for K^+ decays to a muon and invisible particles*, *Phys. Lett. B* **816** (2021) 136259, [[2101.12304](#)].
- [114] **DELPHI Collaboration**, P. Abreu et al., *Search for neutral heavy leptons produced in Z decays*, *Z. Phys. C* **74** (1997) 57–71. [Erratum: *Z.Phys.C* 75, 580 (1997)].
- [115] **BESIII Collaboration**, M. Ablikim et al., *Search for heavy Majorana neutrino in lepton number violating decays of $D \rightarrow K\pi e^+e^+$* , *Phys. Rev. D* **99** (2019), no. 11 112002, [[1902.02450](#)].
- [116] **CMS Collaboration**, A. Tumasyan et al., *Search for long-lived heavy neutral leptons with displaced vertices in proton-proton collisions at $\sqrt{s} = 13$ TeV*, *JHEP* **07** (2022) 081, [[2201.05578](#)].
- [117] **CMS Collaboration**, A. Hayrapetyan et al., *Search for long-lived heavy neutral leptons decaying in the CMS muon detectors in proton-proton collisions at $\sqrt{s} = 13$ TeV*, [2402.18658](#).
- [118] **CMS Collaboration**, A. Hayrapetyan et al., *Search for long-lived heavy neutrinos in the decays of B mesons produced in proton-proton collisions at $\sqrt{s} = 13$ TeV*, *JHEP* **06** (2024) 183, [[2403.04584](#)].

- [119] A. Blondel et al., *Searches for long-lived particles at the future FCC-ee*, *Front. in Phys.* **10** (2022) 967881, [[2203.05502](#)].
- [120] **DsTau (NA65) Collaboration**, S. Aoki et al., *Development of proton beam irradiation system for the NA65/DsTau experiment*, *JINST* **18** (2023), no. 10 P10008, [[2303.13070](#)].
- [121] S. Foroughi-Abari and A. Ritz, *Dark sector production via proton bremsstrahlung*, *Phys. Rev. D* **105** (2022), no. 9 095045, [[2108.05900](#)].
- [122] P. Lo Chiatto and F. Yu, *Consistent Electroweak Phenomenology of a Nearly Degenerate Z' Boson*, [2405.03396](#).
- [123] **Flavour Lattice Averaging Group (FLAG) Collaboration**, Y. Aoki et al., *FLAG Review 2021*, *Eur. Phys. J. C* **82** (2022), no. 10 869, [[2111.09849](#)].
- [124] **HPQCD Collaboration**, J. Harrison, C. Davies, and M. Wingate, *Lattice QCD calculation of the $B_{(s)} \rightarrow D_{(s)}^* \ell \nu$ form factors at zero recoil and implications for $|V_{cb}|$* , *Phys. Rev. D* **97** (2018), no. 5 054502, [[1711.11013](#)].
- [125] **HPQCD Collaboration**, J. Harrison and C. T. H. Davies, *$B_s \rightarrow D_s^*$ form factors for the full q^2 range from lattice QCD*, *Phys. Rev. D* **105** (2022), no. 9 094506, [[2105.11433](#)].
- [126] D. Melikhov and B. Stech, *Weak form-factors for heavy meson decays: An Update*, *Phys. Rev. D* **62** (2000) 014006, [[hep-ph/0001113](#)].
- [127] P. A. Baikov, K. G. Chetyrkin, and J. H. Kuhn, *Order $\alpha_s^4(s)$ QCD Corrections to Z and tau Decays*, *Phys. Rev. Lett.* **101** (2008) 012002, [[0801.1821](#)].
- [128] A. Deur, S. J. Brodsky, and C. D. Roberts, *QCD running couplings and effective charges*, *Prog. Part. Nucl. Phys.* **134** (2024) 104081, [[2303.00723](#)].
- [129] S. Brodsky, P. Hoyer, C. Peterson, and N. Sakai, *The intrinsic charm of the proton*, *Physics Letters B* **93** (1980), no. 4 451–455.
- [130] R. Vogt and S. J. Brodsky, *Charmed hadron asymmetries in the intrinsic charm coalescence model*, *Nucl. Phys. B* **478** (1996) 311–334, [[hep-ph/9512300](#)].
- [131] B. L. Combridge, *Associated Production of Heavy Flavor States in p p and anti-p p Interactions: Some QCD Estimates*, *Nucl. Phys. B* **151** (1979) 429–456.
- [132] B. Andersson, H. U. Bengtsson, and G. Gustafson, *Charm production and the confining force field*, tech. rep., Lund Univ., Lund, 1983.
- [133] B. Andersson, G. Gustafson, G. Ingelman, and T. Sjostrand, *Parton Fragmentation and String Dynamics*, *Phys. Rept.* **97** (1983) 31–145.
- [134] E. Norrbin and T. Sjostrand, *Production mechanisms of charm hadrons in the string model*, *Phys. Lett. B* **442** (1998) 407–416, [[hep-ph/9809266](#)].
- [135] E. Braaten, Y. Jia, and T. Mehen, *The Leading particle effect from heavy quark recombination*, *Phys. Rev. Lett.* **89** (2002) 122002, [[hep-ph/0205149](#)].
- [136] P. Gao and B.-Q. Ma, *The Leading particle effect from light quark fragmentation in charm hadroproduction*, *Eur. Phys. J. C* **50** (2007) 603–608, [[hep-ph/0703133](#)].
- [137] **E791 Collaboration**, E. M. Aitala et al., *Asymmetries between the production of D_s^- and D_s^+ mesons from 500-GeV/c π^- nucleon interactions as functions of $x(F)$ and $p - \text{transverse}^2$* , *Phys. Lett. B* **411** (1997) 230–236, [[hep-ex/9708040](#)].

- [138] **WA89 Collaboration**, M. I. Adamovich et al., *Charge asymmetries for D , $D(s)$ and $\Lambda(c)$ production in Sigma- nucleus interactions at 340-GeV/c*, *Eur. Phys. J. C* **8** (1999) 593–601, [[hep-ex/9803021](#)].
- [139] J. R. Christiansen and P. Z. Skands, *String Formation Beyond Leading Colour*, *JHEP* **08** (2015) 003, [[1505.01681](#)].
- [140] C. Bierlich, G. Gustafson, L. Lönnblad, and A. Tarasov, *Effects of Overlapping Strings in pp Collisions*, *JHEP* **03** (2015) 148, [[1412.6259](#)].
- [141] C. Bierlich, P. Ilten, T. Menzo, S. Mrenna, M. Szewc, et al., *Reweighting Monte Carlo Predictions and Automated Fragmentation Variations in Pythia 8*, *SciPost Phys.* **16** (2024) 134, [[2308.13459](#)].
- [142] **NNPDF Collaboration**, R. D. Ball, A. Candido, J. Cruz-Martinez, S. Forte, T. Giani, et al., *Evidence for intrinsic charm quarks in the proton*, *Nature* **608** (2022), no. 7923 483–487, [[2208.08372](#)].
- [143] **NNPDF Collaboration**, R. D. Ball, A. Candido, J. Cruz-Martinez, S. Forte, T. Giani, et al., *The intrinsic charm quark valence distribution of the proton*, [2311.00743](#).
- [144] A. Gelman, J. Hwang, and A. Vehtari, *Understanding predictive information criteria for bayesian models*, 2013.
- [145] A. Vehtari, A. Gelman, and J. Gabry, *Practical bayesian model evaluation using leave-one-out cross-validation and waic*, *Statistics and Computing* **27** (Aug., 2016) 1413–1432.
- [146] A. Vehtari, D. Simpson, A. Gelman, Y. Yao, and J. Gabry, *Pareto smoothed importance sampling*, 2024.
- [147] J. Jerhot, *Hidden sector searches with fixed-target experiments*. PhD thesis, Louvain U., Louvain U., CP3, 2023.
- [148] R. Brun, F. Rademakers, P. Canal, A. Naumann, O. Couet, et al., *root-project/root: v6.18/02*, .
- [149] C. Bierlich et al., *A comprehensive guide to the physics and usage of PYTHIA 8.3*, *SciPost Phys. Codeb.* **2022** (2022) 8, [[2203.11601](#)].
- [150] R. Mertig, M. Böhm, and A. Denner, *Feyn calc - computer-algebraic calculation of feynman amplitudes*, *Computer Physics Communications* **64** (1991), no. 3 345–359.
- [151] M. Drewes, J. Hajer, J. Klaric, and G. Lanfranchi, *NA62 sensitivity to heavy neutral leptons in the low scale seesaw model*, *JHEP* **07** (2018) 105, [[1801.04207](#)].